arXiv:2202.09106v2 [hep-ex] 30 May 2022

Measurement of the charm mixing parameter $y_{CP} - y_{CP}^{K\pi}$ using two-body D^0 meson decays

LHCb collaboration[†]

Abstract

A measurement of the ratios of the effective decay widths of $D^0 \to \pi^- \pi^+$ and $D^0 \to K^- K^+$ decays over that of $D^0 \to K^- \pi^+$ decays is performed with the LHCb experiment using proton–proton collisions at a centre-of-mass energy of 13 TeV, corresponding to an integrated luminosity of 6 fb^{-1}. These observables give access to the charm mixing parameters $y_{CP}^{\pi\pi} - y_{CP}^{K\pi}$ and $y_{CP}^{KK} - y_{CP}^{K\pi}$, and are measured as

$$y_{CP}^{\pi\pi} - y_{CP}^{K\pi} = (6.57 \pm 0.53 \pm 0.16) \times 10^{-3} ,$$
$$y_{CP}^{KK} - y_{CP}^{K\pi} = (7.08 \pm 0.30 \pm 0.14) \times 10^{-3} ,$$

where the first uncertainties are statistical and the second systematic. The combination of the two measurements is $y_{CP} - y_{CP}^{K\pi} = (6.96 \pm 0.26 \pm 0.13) \times 10^{-3}$, which is four times more precise than the previous world average.

[†]Authors are listed at the end of this paper.

1   Introduction

Neutral charm mesons can change their flavour and turn into their antimeson counterpart before they decay. This phenomenon, known as D^0–$\overline{D}^0$ mixing, does not occur at tree level in the Standard Model and is sensitive to contributions from new particles arising in extensions of the Standard Model. The mass eigenstates of neutral charm mesons can be expressed as a linear combination of their flavour eigenstates, $|D_{1,2}\rangle = p|D^0\rangle \pm q|\overline{D}^0\rangle$, where p and q are complex parameters satisfying $|p|^2 + |q|^2 = 1$. In the limit of charge-parity (CP) symmetry, the relation $|q/p| = 1$ holds. The time evolution of neutral charm meson systems is governed by the effective Hamiltonian $\mathbf{H} = \mathbf{M} - \frac{i}{2}\mathbf{\Gamma}$, where the Hermitian matrices $\mathbf{M}$ and $\mathbf{\Gamma}$ describe $(D^0, \overline{D}^0) \leftrightarrow (D^0, \overline{D}^0)$ dispersive transitions through virtual intermediate states and absorptive transitions through real intermediate states, respectively [1]. The D^0–$\overline{D}^0$ oscillations are described by the two dimensionless parameters $x_{12} = 2|M_{12}/\Gamma|$ and $y_{12} = |\Gamma_{12}/\Gamma|$ [2,3], where $\Gamma = (\Gamma_1 + \Gamma_2)/2$ is the average decay width of the D_1 and D_2 states, and M_{12} (Γ_{12}) is the off-diagonal element of matrix $\mathbf{M}$ ($\mathbf{\Gamma}$). The values of x_{12} and y_{12} are of the order of half a percent and have been measured to be significantly different from zero [4–11].

The non-zero value of y_{12} implies that the time-dependent decay rate of Cabibbo-suppressed $D^0 \to f$ decays, with $f = K^-K^+, \pi^-\pi^+$ final states, is described by an exponential function with an effective decay width $\hat{\Gamma}$ that differs slightly from Γ. The departure from unity of the ratio of the effective decay widths of $D^0 \to \pi^-\pi^+$ and $D^0 \to K^-K^+$ decays over that of $D^0 \to K^-\pi^+$ decays is measured via the observable [1]

$$y_{CP}^f = \frac{\hat{\Gamma}(D^0 \to f) + \hat{\Gamma}(\overline{D}^0 \to f)}{2\Gamma} - 1 \,. \tag{1}$$

The above quantity can be approximated as [12]

$$y_{CP}^f = y_{12} \cos\phi_f^{\Gamma} \,, \tag{2}$$

where $\phi_f^{\Gamma} = \arg\left(\Gamma_{12}A_f/\overline{A}_f\right)$ describes the CP-violating phase difference of the interference between decay amplitudes with and without absorptive mixing [2,3], and A_f ($\overline{A}_f$) is the decay amplitude of a D^0 ($\overline{D}^0$) meson to the final state f. Any deviation of y_{CP}^f from y_{12} would be a sign of CP violation. At the current experimental sensitivity, final-state dependent contributions to y_{CP}^f can be neglected in the limit where the phase ϕ_f^{Γ} is replaced by the universal phase ϕ_2^{Γ}, and $y_{CP} \approx y_{12} \cos\phi_2^{\Gamma}$ [12]. The parameter y_{12} is equal to $|y| \equiv |\Gamma_1 - \Gamma_2|/2\Gamma$ up to second order CP violation effects [12], where the best experimental estimate is $y = (6.30^{+0.33}_{-0.30}) \times 10^{-3}$ [11]. The current world average gives $\phi_2^{\Gamma} = (48^{+29}_{-28})\,\mathrm{mrad}$ [13, 14], implying that $|y_{12} - y_{CP}| < 3 \times 10^{-5}$ at 95% confidence level. Since this upper limit is about one order of magnitude smaller than the current experimental sensitivity on both y_{12} and y_{CP} at LHCb, an accurate measurement of y_{CP} provides important constraints on y_{12}.

The previous measurements of y_{CP} performed by the BABAR [5], Belle [7] and LHCb [9, 15] collaborations use the average decay width of $D^0 \to K^-\pi^+$ and $\overline{D}^0 \to K^+\pi^-$ decays as a proxy to the decay width Γ. It was recently shown in Ref. [13] that the use of this proxy inside the experimental observable of Eq. (1) does not give direct access to y_{CP}^f but rather corresponds to

$$\frac{\hat{\Gamma}(D^0 \to f) + \hat{\Gamma}(\overline{D}^0 \to f)}{\hat{\Gamma}(D^0 \to K^-\pi^+) + \hat{\Gamma}(\overline{D}^0 \to K^+\pi^-)} - 1 \approx y_{CP}^f - y_{CP}^{K\pi} \,. \tag{3}$$

The quantity $y_{CP}^{K\pi}$ is approximately equal to

$$y_{CP}^{K\pi} \approx \sqrt{R_D}\left(x_{12}\cos\phi_2^M \sin\delta_{K\pi} + y_{12}\cos\phi_2^\Gamma \cos\delta_{K\pi}\right) \approx -0.4 \times 10^{-3}\,, \qquad (4)$$

where R_D is the ratio of the branching fractions of the doubly Cabibbo-suppressed $D^0 \to K^+\pi^-$ decay over the Cabibbo-favoured $D^0 \to K^-\pi^+$ decay. The current best experimental estimate is $\sqrt{R_D} = (5.87 \pm 0.02) \times 10^{-2}$ [16]. The phase ϕ_2^M is equal to the phase of M_{12} with respect to its $\Delta U = 2$ dominant contribution, and $\delta_{K\pi}$ is the strong-phase difference between the doubly Cabibbo-suppressed and Cabibbo-favoured decay amplitudes [11]. In the limit of no CP violation and of U-spin symmetry in $D^0 \to K^\mp\pi^\pm$ decays, the approximations $\delta_{K\pi} \approx \pi$ and $y_{CP} - y_{CP}^{K\pi} \approx y_{12}(1 + \sqrt{R_D})$ hold.

The world average value of $y_{CP} - y_{CP}^{K\pi}$ is measured to be $(7.19 \pm 1.13) \times 10^{-3}$ [16]. This paper reports a new measurement of $y_{CP} - y_{CP}^{K\pi}$. The result is obtained from a weighted average of statistically independent measurements with K^-K^+ and $\pi^-\pi^+$ final states, using proton-proton (pp) collision data collected with the LHCb experiment at a centre-of-mass energy of $13\,\mathrm{TeV}$ in the Run 2 data taking period (2015–2018), corresponding to an integrated luminosity of $6\,\mathrm{fb}^{-1}$. The D^0 mesons are required to originate from $D^*(2010)^+ \to D^0\pi_{\mathrm{tag}}^+$ decays, such that their flavour at production is identified by the charge of the tagging pion, π_{tag}^+. The inclusion of charge-conjugate processes is implied throughout. Hereafter the $D^*(2010)^+$ meson is referred to as a D^{*+} meson.

2 LHCb detector

The LHCb detector [17, 18] is a single-arm forward spectrometer covering the pseudo-rapidity range $2 < \eta < 5$, designed for the study of particles containing b or c quarks. The detector includes a high-precision tracking system consisting of a silicon-strip vertex detector surrounding the pp interaction region, a large-area silicon-strip detector located upstream of a dipole magnet with a bending power of about $4\,\mathrm{Tm}$, and three stations of silicon-strip detectors and straw drift tubes placed downstream of the magnet. The tracking system provides a measurement of the momentum, p, of charged particles with a relative uncertainty varying from 0.5% at low momentum to 1.0% at $200\,\mathrm{GeV}/c$. The minimum distance of a track to a primary vertex (PV), the impact parameter (IP), is measured with a resolution of $(15 + 29/p_{\mathrm{T}})\,\mu\mathrm{m}$, where p_{T} is the component of the momentum transverse to the beam, in GeV/c. The LHCb coordinate system is right-handed, with the z axis pointing along the beam axis, y the vertical direction pointing upwards, and x the horizontal direction. The origin corresponds to the nominal pp interaction point. The magnetic field deflects oppositely charged particles in opposite directions along the x axis, inducing potential detection asymmetries. Therefore, the magnet polarity is reversed regularly throughout the data taking to reduce the effects of detection asymmetries. The two polarities are referred to as *MagUp* and *MagDown*. Different types of charged hadrons are distinguished using information from two ring-imaging Cherenkov (RICH) detectors. Photons, electrons and hadrons are identified by a calorimeter system consisting of scintillating-pad and preshower detectors, an electromagnetic and a hadronic calorimeter. Muons are identified by a system composed of alternating layers of iron and multiwire proportional chambers.

The online event selection is performed by a trigger, which consists of a hardware stage followed by a two-level software stage, which applies a full event reconstruction. The

good performance of the online reconstruction allows this measurement to be performed using candidates reconstructed directly at the trigger level [19, 20].

Simulation is used to study the background of secondary D^{*+} candidates from B meson decays (Sect. 5), and to validate the analysis procedure. The pp collisions are generated with PYTHIA [21] with a specific LHCb configuration [22]. The interaction of the simulated particles with the detector material are described using the GEANT4 toolkit [23, 24]. Decays of unstable particles are described by EVTGEN [25], in which final state radiation is generated using PHOTOS [26]. In addition, fast simulation is generated with the RAPIDSIM package [27]. RAPIDSIM simulations allow for a first validation of the analysis procedure (Sect. 6), and for a description of the background under the D^0 mass peak (Sect. 8).

3 Measurement strategy

The parameters $y_{CP}^f - y_{CP}^{K\pi}$ are measured from the decay-time ratios $R^f(t)$ of $D^0 \to f$ over $D^0 \to K^-\pi^+$ signal yields as a function of the reconstructed D^0 decay time, t, assuming all D^0 mesons are produced at the PV,

$$R^f(t) = \frac{N(D^0 \to f, t)}{N(D^0 \to K^-\pi^+, t)} \propto e^{-(y_{CP}^f - y_{CP}^{K\pi})\,t/\tau_{D^0}} \frac{\varepsilon(f, t)}{\varepsilon(K^-\pi^+, t)} \,, \tag{5}$$

where $\tau_{D^0} = (410.1 \pm 1.5)\,\text{fs}$ is the measured lifetime of the D^0 meson [1], and $\varepsilon(h^- h'^+, t)$, with $h^{(')\pm}$ denoting $K^\pm$ or $\pi^\pm$, is the time-dependent efficiency for the considered final state. Equation (5) indicates that the access to $y_{CP}^f - y_{CP}^{K\pi}$ using an exponential fit is affected by the presence of both efficiencies. In this paper, the term *numerator (denominator) decay* refers to the decay quoted in the numerator (denominator) of the ratio $R^f(t)$. The time-dependent efficiency can be written as the product of two distinct components. The selection efficiency is related to requirements applied at various stages of the LHCb data acquisition system, while the detection efficiency arises from the interaction of the charged kaons and pions with the LHCb detector. The time dependence of the efficiencies of the numerator and denominator decays differs because of their different final states, and could bias the measurement if not accounted for. The analysis strategy consists of equalising the selection efficiencies and then the detection efficiencies of the numerator and denominator decays. Their combined effects cancel out in the decay time ratio, such that $y_{CP}^f - y_{CP}^{K\pi}$ can be measured without additional corrections. Both steps are performed using data-driven methods detailed in the following paragraphs.

The selection efficiencies of $D^0 \to f$ and $D^0 \to K^-\pi^+$ decays mainly differ because of the different masses of their final-state particles, leading to distinct kinematic distributions of the final state particles of the D^0 candidate in the laboratory (lab) frame. The parent D^0 meson has a momentum p and decay angle $\theta^*(h^-)$ that are independent of the pair of the final states considered in this analysis. The angle $\theta^*(h^-)$ is defined as the angle between the momentum of the negatively charged final state particle h^- in the centre-of-mass frame of the D^0 meson and the D^0 momentum in the lab frame. To obtain equal acceptance for both decays, we require that each D^0 candidate selected in one final state would also pass the selection requirements for the other final state with the same D^0 kinematic properties. A *kinematic matching procedure* has been developed for this purpose [28]. It consists of an event-by-event analytical transformation, which matches the final-state kinematic
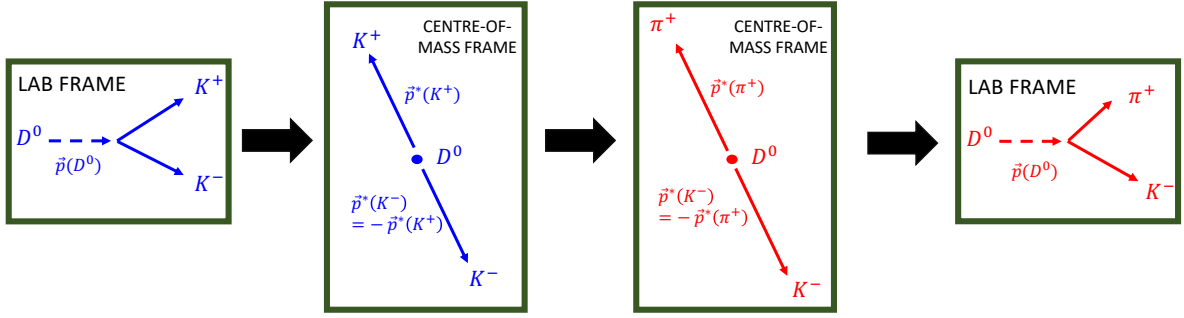
Figure 1: Sketch of a $D^0 \to K^- K^+$ to $D^0 \to K^- \pi^+$ matching.

variables of one decay to the other. To match the kinematics of a $D^0 \to K^- K^+$ decay to a $D^0 \to K^- \pi^+$ decay (sketched in Fig. 1), a boost to the centre-of-mass frame of the D^0 candidate is performed, such that both final-state particle momenta have equal magnitude,

$$|\vec{p}^*| = \frac{\sqrt{(m_{D^0}^2 - (m_{K^+} - m_{K^-})^2)(m_{D^0}^2 - (m_{K^+} + m_{K^-})^2)}}{2m_{D^0}} \,, \qquad (6)$$

where m_i refers to the masses of the particles. By substituting m_{K^+} with m_{π^+}, $|p^*|$ changes from $791\,\mathrm{MeV}/c$ to $861\,\mathrm{MeV}/c$, and a $D^0 \to K^- \pi^+$ state with identical kinematic properties is generated. The use of the $K^- \pi^+$ kinematics in the lab frame derived from this procedure (referred to as *matched* kinematic quantities) ensures that both the matched $D^0 \to K^- K^+$ and the target $D^0 \to K^- \pi^+$ decays cover the same kinematic phase space.

The correction of the difference of detection efficiencies is treated with the *kinematic weighting procedure*, which is performed after the kinematic matching. The procedure consists of weighting the p, p_{T} and η distributions of the D^{*+} meson and both matched final-state particles of one of the decays to the distributions of the other decay. The procedure is performed using a gradient-boosted-reweighting algorithm from the `hep_ml` library [29].

The analysis procedure is validated with three distinct methods. First, a measurement of $y_{CP}^{KK} - y_{CP}^{K\pi}$ is performed making use of fast simulation samples generated with the RAPIDSIM package, where strong variations of the time-dependent efficiencies as a function of the kinematic variables are introduced to test the robustness of the procedure. Second, the measurement is performed making use of large fully simulated samples. Finally, the procedure is validated with LHCb data through a study of a cross-check observable, $R^{CC}(t)$, built from the time-dependent ratio of the yields of $D^0 \to \pi^- \pi^+$ and $D^0 \to K^- K^+$ decays,

$$R^{CC}(t) = \frac{N(D^0 \to \pi^- \pi^+, t)}{N(D^0 \to K^- K^+, t)} \propto e^{-y_{CP}^{CC} \, t/\tau_{D^0}} \frac{\varepsilon(\pi^- \pi^+, t)}{\varepsilon(K^- K^+, t)} \,, \qquad (7)$$

where the parameter y_{CP}^{CC} is expected to be compatible with zero, since the final-state dependent part of y_{CP} is negligible. The observable $R^{CC}(t)$ benefits from the fact that both final state tracks are different for numerator and denominator decays, increasing the biasing effects from their corresponding efficiencies.

The data samples are contaminated by the presence of three noticeable background contributions. The first is the combinatorial background, which is subtracted by means of

4

a fit to the distribution of $\Delta m = m(h^- h^+ \pi_{\text{tag}}^+) - m(h^- h^+)$, where $m(h^- h^+ \pi_{\text{tag}}^+)$ is the mass of the D^{*+} candidate and $m(h^- h^+)$ that of the D^0 candidate. The second background contribution comes from D^{*+} mesons that are not produced at the PV but from the decay of B mesons. The effect of such secondary decays on the measurement is accounted by including their presence in the fit model of Eq. (5). The treatment of the combinatorial background and of secondary decays is detailed in Sect. 5. A third background contribution is related to the presence of partially reconstructed or misreconstructed $D^{*+} \to D^0 \pi^+$ decays. A systematic uncertainty is estimated to cover their impact on the measurement and is discussed in Sect. 8.

4 Candidate selection

The $D^{*+} \to (D^0 \to h^- h'^+) \pi_{\text{tag}}^+$ decays are reconstructed at the trigger level. At the hardware stage, the trigger decision is required to be based on particles independent of the signal candidates, as requiring a decision depending on the signal candidates would degrade the performance of the kinematic matching procedure. Both software trigger stages were specifically designed to minimise the biasing effects to the decay time ratio $R^f(t)$, as detailed in Ref. [30]. This is achieved by avoiding requirements on kinematic variables of the final-state particles that are strongly correlated with the D^0 decay time. Candidate D^0 mesons are constructed from $h^- h'^+$ pairs which have a distance of closest approach of less than $100\,\mu$m, form a vertex with a χ^2 per degree of freedom less than ten, and have an invariant mass in the interval $[1804, 1924]\,$MeV$/c^2$. The reconstructed D^0 decay time is required to be higher than $0.6\,\tau_{D^0}$. The angle between the D^0 momentum vector and the vector connecting the D^0 decay vertex and the PV is required to be less than $8°$, and the D^0 transverse momentum larger than $2\,$GeV$/c$. Both final-state particles are required to have an individual transverse momentum above $800\,$MeV$/c$, and at least one of these must have a transverse momentum exceeding $1200\,$MeV$/c$. Furthermore, their individual absolute momenta are required to be higher than $5\,$GeV$/c$. Finally, based on the information provided by the RICH detectors, the final-state candidates are assigned a pion or kaon mass. To remove statistical correlations between the $y_{CP}^{\pi\pi} - y_{CP}^{K\pi}$ and $y_{CP}^{KK} - y_{CP}^{K\pi}$ measurements related to the common $K^- \pi^+$ final state, the $D^0 \to K^- \pi^+$ sample is split into two statistically independent samples. Since three times more $D^0 \to K^- K^+$ than $D^0 \to \pi^- \pi^+$ signal candidates are selected, the $D^0 \to K^- \pi^+$ sample is split accordingly for the $y_{CP}^{\pi\pi} - y_{CP}^{K\pi}$ and $y_{CP}^{KK} - y_{CP}^{K\pi}$ measurements.

In the offline selection, all kaon and pion tracks are required to have a pseudorapidity in the range 2.0 to 4.2 to remove particles traversing regions of high material density. The D^0 flight distance in the $x - y$ plane is required to be less than $4\,$mm to remove D^{*+} candidates produced from interactions with the detector material. The z-coordinate of the D^0 decay vertex is required not to exceed a distance of $20\,$cm from the pp interaction point to remove residual background reconstructed at larger distances. The invariant mass of the D^0 meson is requested to lie within the interval $[1851, 1880]\,$MeV$/c^2$, corresponding to about twice the resolution around the known D^0 mass [1]. A large fraction of secondary D^{*+} mesons is removed by demanding that the measured IP of D^0 mesons does not exceed $50\,\mu$m (see Sect. 5). This requirement is also very effective at removing combinatorial background. The resolution on the D^0 decay time is improved by performing a kinematic fit [31] in which the D^{*+} candidate is required to originate from the PV. The reconstructed
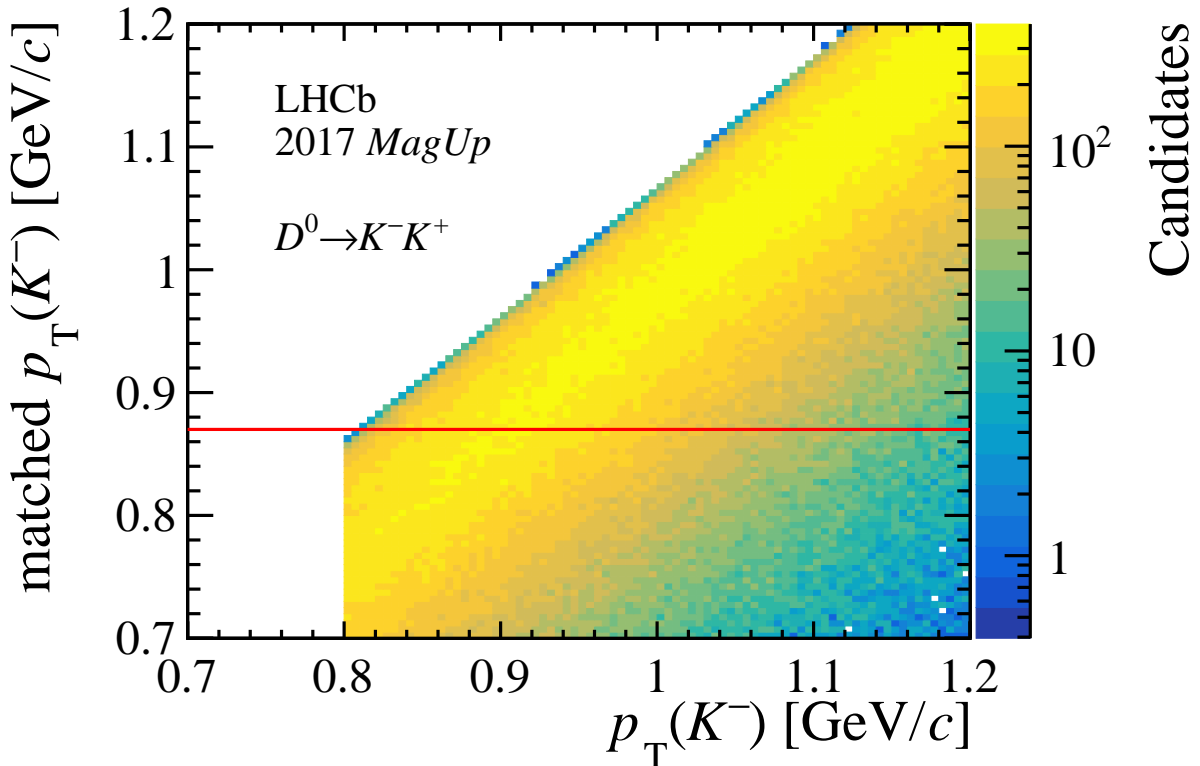
Figure 2: Matched versus original transverse momenta for the matching of a K^- to a π^- particle, related to the y_{CP}^{CC} measurement. The red line represents the requirement applied to the data sample, where candidates below the line are rejected. The plot is obtained with the 2017 *MagUp* sample.

D^0 decay time is selected in the interval $[1.0, 8.0]\tau_{D^0}$. The lower bound is chosen to minimise biasing effects related to the differences of the time resolution between the three D^0 decay channels, and to avoid significant combinatorial background from the PV. The higher bound is set to minimise the contribution from secondary decays, the fraction of which increases as a function of D^0 decay time.

The kinematic matching procedure is then performed for the selected candidates, as detailed in Sect. 3. Figure 2 illustrates the transverse momentum of the K^- candidate of a $D^0 \to K^- K^+$ decay matched to the π^- candidate of a $D^0 \to \pi^- \pi^+$ decay. The trigger selection requirement on the kaon transverse momentum at $0.8\,\text{GeV}/c$ is visible as a sharp cut on the x axis. A requirement on the matched transverse momentum of the kaon, visible on the y axis, to be larger than $0.87\,\text{GeV}/c$, is effectively tighter than the trigger requirement applied on the $D^0 \to K^- K^+$ candidates. The application of this tighter requirement in the selection of both the matched $D^0 \to K^- K^+$ and the $D^0 \to \pi^- \pi^+$ candidates ensures that both decays are selected with the same efficiency profile. Similarly, for each kinematic variable of the D^0 candidates, a tightened requirement on the matched variable is applied to the matched and target decays. For the three measurements described in this paper, the matched (target) decay is that with the smallest (largest) momentum of the final-state particles in the D^0 rest frame, which consists in matching kaon to

pion candidates, allowing for the minimal loss of statistical precision. Hence, for the y_{CP}^{CC} measurement, the $D^0 \to K^- K^+$ decay is matched to the $D^0 \to \pi^- \pi^+$ decay; for the $y_{CP}^{KK} - y_{CP}^{K\pi}$ measurement, the $D^0 \to K^- K^+$ decay is matched to the $D^0 \to K^- \pi^+$ decay; finally, for the $y_{CP}^{\pi\pi} - y_{CP}^{K\pi}$ measurement, the $D^0 \to K^- \pi^+$ decay is matched to the $D^0 \to \pi^- \pi^+$ decay. An additional requirement on matched quantities is that the variable $\tilde{\chi}^2_{\mathrm{IP}} = \mathrm{IP}^2/(11.6 + 23.4/p_{\mathrm{T}})^2$, where p_{T} is expressed in GeV/c and IP in µm, to be larger than 6.0 [32]. This allows the combinatorial background in the data sample to be reduced further. The data sample is split into 22 intervals of D^0 decay time of equal population, with the exception of the four intervals with the largest decay times containing half of the population of the others.

Following the offline and matching requirements, about 6% of the $D^0 \to K^- K^+$ and $D^0 \to \pi^- \pi^+$ and 3.5% of the $D^0 \to K^- \pi^+$ candidates are combined with multiple π^+_{tag} candidates to form D^{*+} meson candidates. When multiple candidates are present in the event, one is selected randomly.

5 Mass fit and dominant background contributions

The Δm distributions of all three decay channels are shown in Fig. 3 for the combined data set. A binned maximum-likelihood fit is applied to the Δm distribution to separate signal from combinatorial background arising predominantly from the association of a D^0 meson with a random π^+_{tag} candidate from the pp interaction. The signal is fitted with the sum of three Gaussian functions and a Johnson SU function [33]. The combinatorial background is fitted with the empirical model

$$\mathcal{P}_{\mathrm{BKG}}(\Delta m | m_0, \alpha) = \frac{1}{\mathcal{I}_B} \Delta m \cdot \sqrt{\frac{\Delta m^2}{m_0^2} - 1} \cdot \exp\left(-\alpha \left(\frac{\Delta m^2}{m_0^2} - 1\right)\right), \qquad (8)$$

where m_0 and α are free parameters, and $\mathcal{I}_B$ is a normalisation constant. In the Δm distribution, a signal region is defined in the interval $[144.45, 146.45]$ MeV/c^2 and a sideband region in the interval $[150, 154]$ MeV/c^2. The contribution from the residual background in the signal region is estimated from the sideband region and subtracted with a dedicated procedure. The fitting of the Δm distribution is performed independently for each D^0 flavour, year and magnet polarity, and in each of the 22 intervals of D^0 decay time. In the signal region, the time-integrated signal purities are equal to 98%, 96%, and 95% for the $D^0 \to K^- \pi^+$, $D^0 \to K^- K^+$ and $D^0 \to \pi^- \pi^+$ channels, respectively, and the time-integrated signal yields amount to 70 million, 18 million, and 6 million decays. The fits to the Δm distributions of all three decay channels are displayed in Fig. 3.

The data samples are also contaminated by the presence of secondary D^{*+} mesons, which are not produced at the PV but from B meson decays. Since the reconstructed D^0 decay time is calculated as $t = l \cdot m(D^0)/p(D^0)$, where l is the measured distance between the PV and the decay vertex of the D^0 meson, t is overestimated for secondary candidates since l is affected by the flight distance of B mesons. The IP of the corresponding D^0 candidates is usually different from zero, as opposed to D^0 candidates from prompt D^{*+} decays. Hence, requesting the IP of D^0 candidates not to exceed 50 µm allows a significant fraction of secondary D^{*+} mesons, $f_{\mathrm{sec}}(t)$, defined as the time-dependent ratio of the number of D^0 mesons from secondary decays over the total, to be rejected from the data sample. To account for the residual contamination of secondary D^{*+} candidates, the ratio
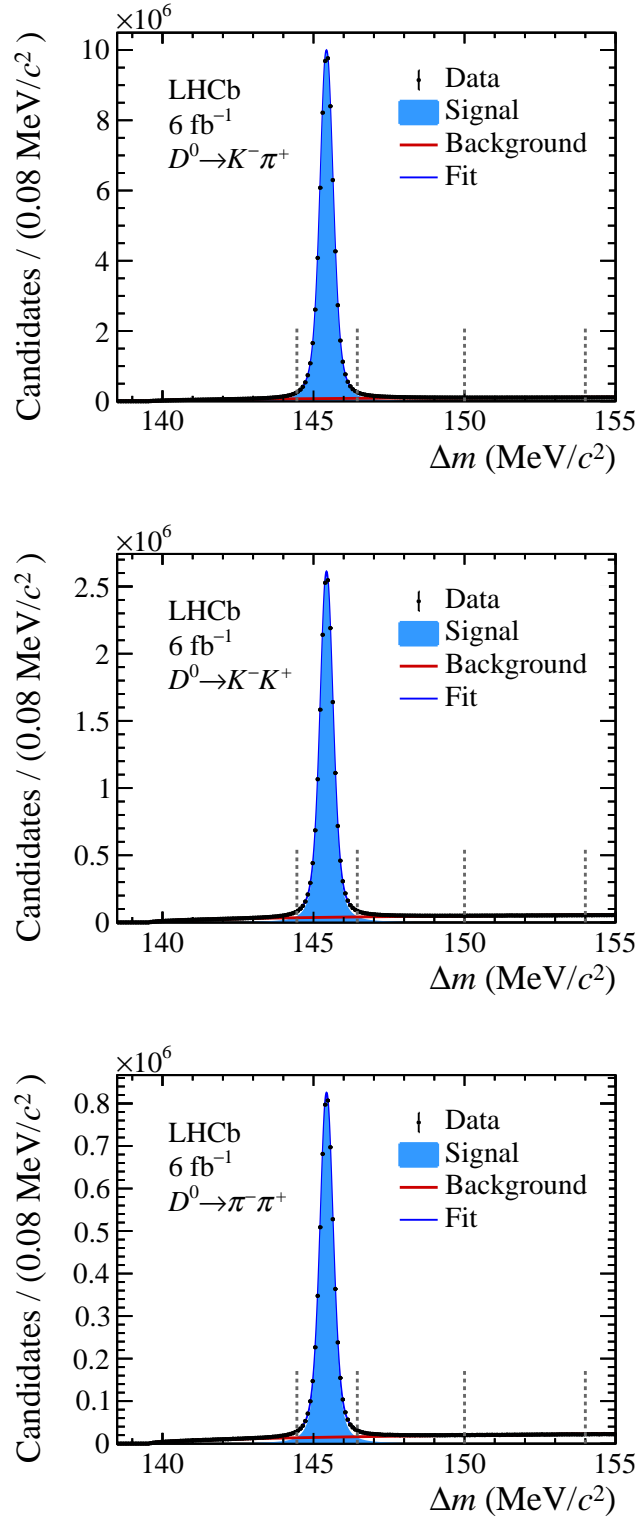
Figure 3: Distributions of Δm for the (top) $D^0 \to K^-\pi^+$, (centre) $D^0 \to K^-K^+$, and (bottom) $D^0 \to \pi^-\pi^+$ decay channels for the combined data sample. The signal and sideband regions employed to subtract the combinatorial background are delimited by the dashed vertical lines. The sum of the fit projections are overlaid.
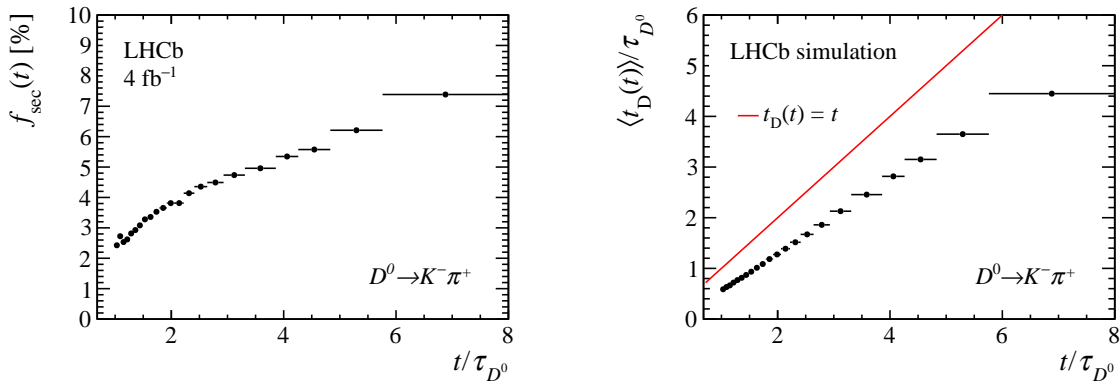
Figure 4: (Left) fraction and (right) average true D^0 decay time of secondary decays as a function of the reconstructed D^0 decay time, in units of the average D^0 lifetime.

$R^f(t)$ is separated according to its prompt and secondary components, $R^f_{\text{prompt}}(t)$ and $R^f_{\text{sec}}(t)$, as

$$R^f(t) = (1 - f_{\text{sec}}(t))R^f_{\text{prompt}}(t) + f_{\text{sec}}(t)R^f_{\text{sec}}(t) \,. \tag{9}$$

The decay time ratio of D^0 mesons from secondary D^{*+} decays is expressed as

$$R^f_{\text{sec}}(t) \propto e^{-(y^f_{CP} - y^{K\pi}_{CP})\langle t_D(t)\rangle/\tau_{D^0}} \,, \tag{10}$$

where $\langle t_D(t)\rangle$ is the average true D^0 decay time $\langle t_D\rangle$ as a function of the reconstructed D^0 decay time t. The quantities $f_{\text{sec}}(t)$ and $\langle t_D(t)\rangle$ are determined using data and simulated samples of $D^0 \to K^-\pi^+$ decays generated separately for prompt D^{*+} decays and through the expected mixture of B^0 and B^+ meson decays to D^{*+} candidates. The kinematic distributions of the simulation samples are weighted to those of data samples to account for kinematic discrepancies. The fraction $f_{\text{sec}}(t)$ is obtained by fitting the distribution of IP(D^0) in data in each interval of t using simulation-based templates of IP(D^0) from prompt and secondary decays. The values of $f_{\text{sec}}(t)$ are measured to increase from about 2% to 7% across the studied D^0 decay time range. The quantity $\langle t_D(t)\rangle$ is determined from the simulated sample of secondary decays. The obtained values of $f_{\text{sec}}(t)$ and $\langle t_D(t)\rangle$ are shown in Fig. 4.

6 Analysis validation with simulation

The kinematic matching procedure is validated with the use of RAPIDSIM simulation. Signal candidates of prompt $D^{*+} \to (D^0 \to K^-K^+)\pi^+_{\text{tag}}$ and $D^{*+} \to (D^0 \to K^-\pi^+)\pi^+_{\text{tag}}$ decays are generated without D^0–$\overline{D}^0$ mixing. The simulation samples are subjected to selection criteria representative of the trigger. These include requirements on momentum and IP-related quantities, which are strongly correlated with the D^0 decay time and induce substantial differences between the selection efficiency profiles of $D^0 \to K^-K^+$ and $D^0 \to K^-\pi^+$ decays at low D^0 decay time. The kinematic matching procedure is then applied to equalise the selection efficiencies of $D^0 \to K^-K^+$ and $D^0 \to K^-\pi^+$ decays. Following this correction, a fit to the decay time ratio $R^{KK}(t)$ gives $y^{KK}_{CP} - y^{K\pi}_{CP} = (0.17 \pm 0.19) \times 10^{-3}$, compatible with the expected value of zero. This study demonstrates that the kinematic

matching procedure corrects effectively for the kinematic differences between the two decays.

The analysis procedure is further validated with full simulation. Large signal yields of 50 million $D^0 \to K^-\pi^+$, 33 million $D^0 \to K^-K^+$ and 11 million $D^0 \to \pi^-\pi^+$ decays are obtained by generating the particles of the studied decay chain without the full underlying event. The analysis procedure detailed in Sect. 4 is applied to all three decay channels independently for each year and magnet polarity to account for potential differences between the data taking conditions, and the results are combined as a final step. Following the application of the kinematic matching and weighting procedures, the parameters are measured to be

$$y_{CP}^{CC} = (0.15 \pm 0.36) \times 10^{-3}\,,$$
$$y_{CP}^{\pi\pi} - y_{CP}^{K\pi} = (0.17 \pm 0.43) \times 10^{-3}\,,$$
$$y_{CP}^{KK} - y_{CP}^{K\pi} = (0.10 \pm 0.24) \times 10^{-3}\,,$$

where the uncertainties are smaller than the statistical uncertainties expected in data. All three results are compatible with zero. This is expected since D^0–$\overline{D}^0$ mixing has not been simulated. This result validates the analysis procedure with simulation.

7 Results

Both matching and weighting procedures are employed to perform the measurements of y_{CP}^{CC}, $y_{CP}^{\pi\pi} - y_{CP}^{K\pi}$ and $y_{CP}^{KK} - y_{CP}^{K\pi}$ for each year and magnet polarity of the LHCb Run 2 data set. Figure 5 presents the normalised distributions of the D^0 decay angle prior to any kinematic correction (raw) and after the application of both kinematic matching and weighting procedures. The two correction procedures significantly improve the agreement between the distributions. The agreement is also verified to be good for a series of additional kinematic variables.

The parameters y_{CP}^{CC}, $y_{CP}^{KK} - y_{CP}^{K\pi}$, and $y_{CP}^{\pi\pi} - y_{CP}^{K\pi}$ are determined from a χ^2 fit to the corresponding time-dependent $R^f(t)$ ratios. The results of the measurements are presented in Fig. 6, where χ^2 fits with a constant function are performed to determine the averages over all data samples. The results of these fits are reported in Table 1. The raw measurements have good compatibility among the different years and magnet polarities. This indicates uniform performance of the trigger and offline selections, which do not include effects substantially biasing the measurements. The kinematic matching procedure shifts the average value of y_{CP}^{CC} by $(-0.96\pm0.21)\times 10^{-3}$, $y_{CP}^{\pi\pi} - y_{CP}^{K\pi}$ by $(-0.67\pm0.21)\times 10^{-3}$, and $y_{CP}^{KK} - y_{CP}^{K\pi}$ by $(+0.50 \pm 0.12) \times 10^{-3}$. The shifts of $y_{CP}^{\pi\pi} - y_{CP}^{K\pi}$ and $y_{CP}^{KK} - y_{CP}^{K\pi}$ are compatible in magnitude but opposite in sign, as expected given the difference in the nature of the final states in the numerators of their respective decay time ratios. The shifts of y_{CP}^{CC} are measured to be about twice those of $y_{CP}^{\pi\pi} - y_{CP}^{K\pi}$, expected from the fact that $R^{CC}(t)$ probes the decay time ratio of final states in which both particles have different masses. The kinematic weighting shifts the values of y_{CP}^{CC} and $y_{CP}^{f} - y_{CP}^{K\pi}$ by a few 10^{-4} towards negative values. Finally, the use of the fit model of Eq. (9), which takes into account the presence of secondary decays, shifts the average values of $y_{CP}^{f} - y_{CP}^{K\pi}$ by about $+0.1 \times 10^{-3}$.

All three measurements have individual fits of good quality and are found to be compatible among years and magnet polarities. Following all correction procedures and
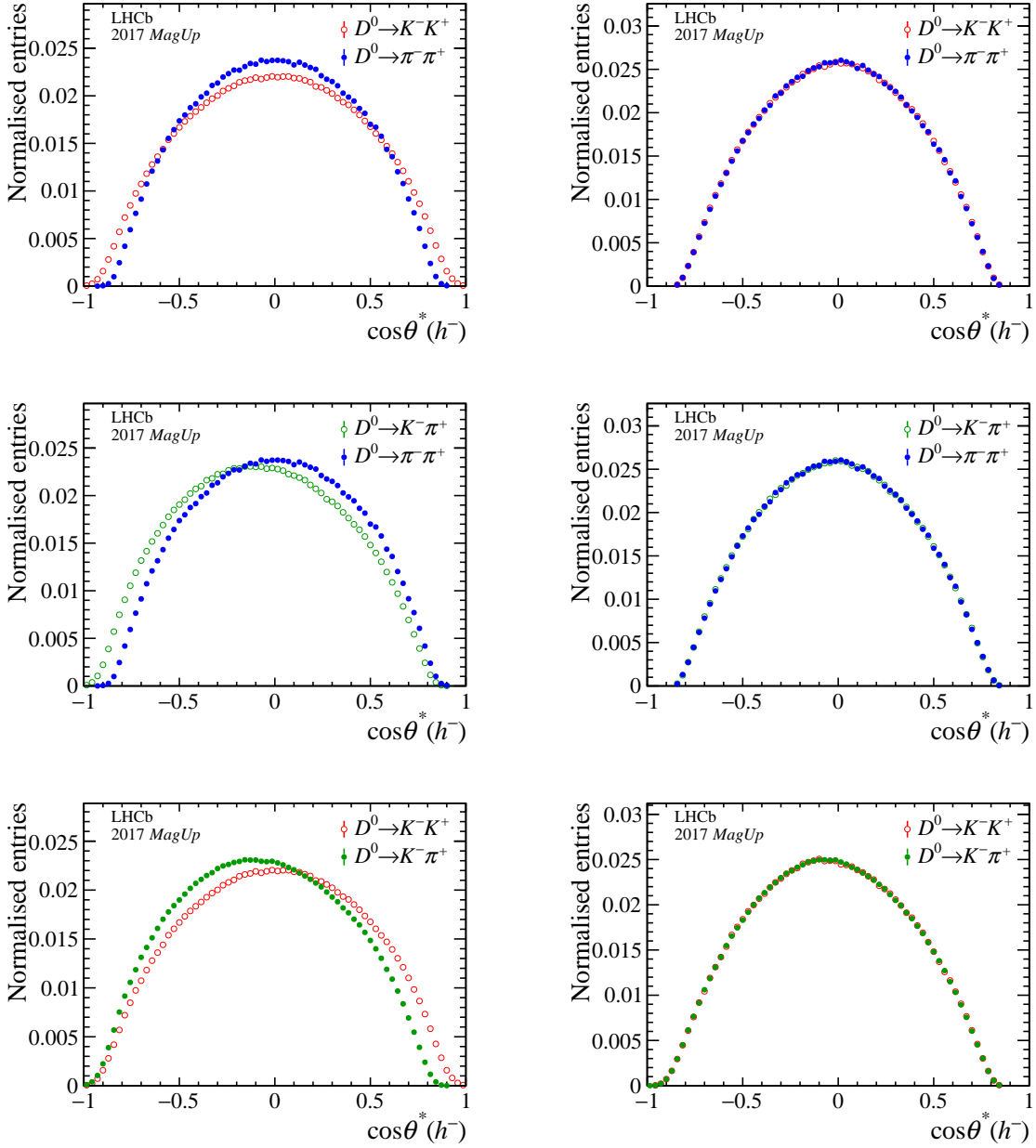
Figure 5: (Left) normalised distributions of the D^0 decay angle $\cos\theta^*(h^-)$ in the raw condition, and (right) following both kinematic matching and reweighting procedures. The distributions are shown for the (top) y_{CP}^{CC}, (middle) $y_{CP}^{\pi\pi} - y_{CP}^{K\pi}$ and (bottom) $y_{CP}^{KK} - y_{CP}^{K\pi}$ measurements. The plots are obtained with the 2017 *MagUp* sample.

the use of the fit model of Eq. (9), which includes secondary decays, the average values are measured to be

$$y_{CP}^{CC} = (-0.44 \pm 0.53) \times 10^{-3} \,,$$
$$y_{CP}^{\pi\pi} - y_{CP}^{K\pi} = (6.57 \pm 0.53) \times 10^{-3} \,,$$
$$y_{CP}^{KK} - y_{CP}^{K\pi} = (7.08 \pm 0.30) \times 10^{-3} \,,$$

where the uncertainties are only statistical. The value of y_{CP}^{CC} is measured to be compatible

Table 1: Results of the χ^2 fits of Fig. 6 for each correction procedure. The results are shown in units of 10^{-3}, while the values in parenthesis correspond to the χ^2 of the fits, where the number of degrees of freedom is 7 for all measurements.

	y_{CP}^{CC}	$y_{CP}^{KK} - y_{CP}^{K\pi}$	$y_{CP}^{KK} - y_{CP}^{K\pi}$
Raw	0.68 ± 0.47 (7.9)	7.48 ± 0.48 (5.5)	6.64 ± 0.27 (6.6)
Matching	-0.28 ± 0.52 (8.3)	6.80 ± 0.52 (2.9)	7.14 ± 0.29 (5.5)
Matching + Weighting	-0.43 ± 0.52 (9.0)	6.44 ± 0.52 (2.8)	6.94 ± 0.29 (5.9)
Matching + Weighting + Fit with secondaries	-0.44 ± 0.53 (9.0)	6.57 ± 0.53 (2.8)	7.08 ± 0.30 (5.9)

with zero within one standard deviation (σ), validating the cross-check measurement with data. Figure 7 shows the distributions of $R^{\pi\pi}(t)$ and $R^{KK}(t)$ using the full data set, with Eq. (9) overlaid, computed using the average values of $y_{CP}^{\pi\pi} - y_{CP}^{K\pi}$ and $y_{CP}^{KK} - y_{CP}^{K\pi}$.

8 Systematic uncertainties

Although the analysis procedure is designed to minimise systematic uncertainties on $y_{CP}^{f} - y_{CP}^{K\pi}$, several sources of possible bias in the results remain and are evaluated. The first source of systematic uncertainty arises from the subtraction of the combinatorial background, which relies on the assumption that the kinematic properties of combinatorial background candidates are identical in the signal and in the sideband interval of the Δm distribution. A systematic uncertainty on this assumption is assigned by repeating the measurement using three alternative sideband regions, namely $[140.5, 142]$, $[149, 152]$ and $[152, 155]\,\mathrm{MeV}/c^2$. An additional source of systematic uncertainty is assigned by propagating the uncertainties on the combinatorial background subtraction. The combined systematic uncertainty is measured to be 0.12×10^{-3} for $y_{CP}^{\pi\pi} - y_{CP}^{K\pi}$ and 0.07×10^{-3} for $y_{CP}^{KK} - y_{CP}^{K\pi}$, the first being higher due to larger combinatorial background level and smaller size of the $D^0 \to \pi^- \pi^+$ sample.

A second source of systematic uncertainty is related to the presence of partially reconstructed or misreconstructed $D^{*+} \to D^0 \pi^+$ decays. These decays are referred to as peaking background since they show a peaking structure in the Δm distribution. For each decay channel, the peaking background contributions are studied with RAPIDSIM simulation. The simulation samples are used as templates to fit the D^0 mass distributions, from which the fraction of peaking background candidates is determined in the signal region. In the $D^0 \to \pi^- \pi^+$ channel, the $D^0 \to \pi^- e^+ \nu_e$ and $D^0 \to \pi^- \mu^+ \nu_\mu$ background components are significant in the D^0 signal mass region. The background fraction is measured as 3.5×10^{-4}. In the $D^0 \to K^- \pi^+$ channel, the $D^0 \to \pi^- \pi^+ \pi^0$, $D^0 \to K^- e^+ \nu_e$ and $D^0 \to K^- \mu^+ \nu_\mu$ background contributions are dominant, and the background fraction is estimated as 8.9×10^{-4}. Finally, in the $D^0 \to K^- K^+$ channel, the dominant background sources come from the $D^0 \to K^- \pi^+ \pi^0$, $D^0 \to K^- e^+ \nu_e$ and $D^0 \to K^- \mu^+ \nu_\mu$ decay channels.
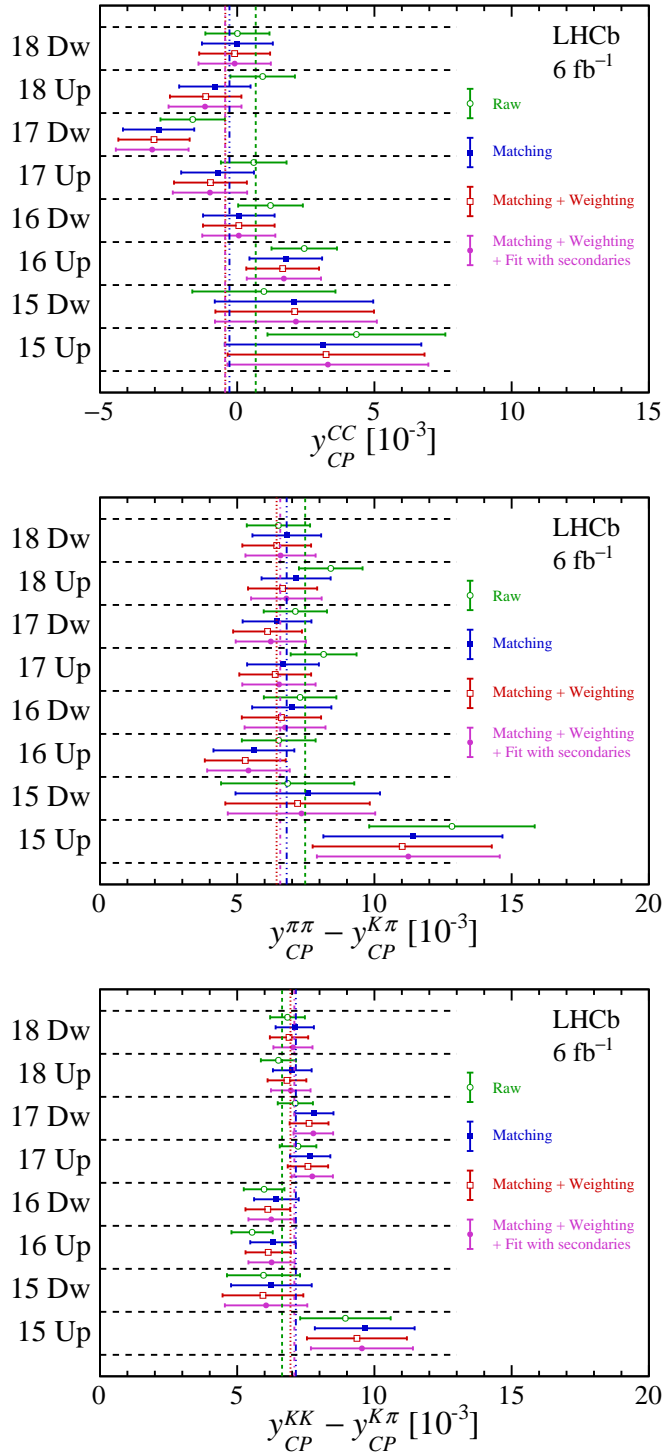
Figure 6: Results for (top) y_{CP}^{CC}, (centre) $y_{CP}^{\pi\pi} - y_{CP}^{K\pi}$ and (bottom) $y_{CP}^{KK} - y_{CP}^{K\pi}$. The measurements employing raw data, and following both matching and weighting conditions are shown in green, blue and red, respectively. The measurements in purple employ the fit model where the presence of secondary decays is considered. The dashed vertical lines correspond to χ^2 fits, used to determine the average values other all subsamples. In the y-axis labels, the data-taking year is abbreviated with the last two digits only and the magnet polarity *MagUp* (*MagDown*) is abbreviated as "Up" ("Dw").
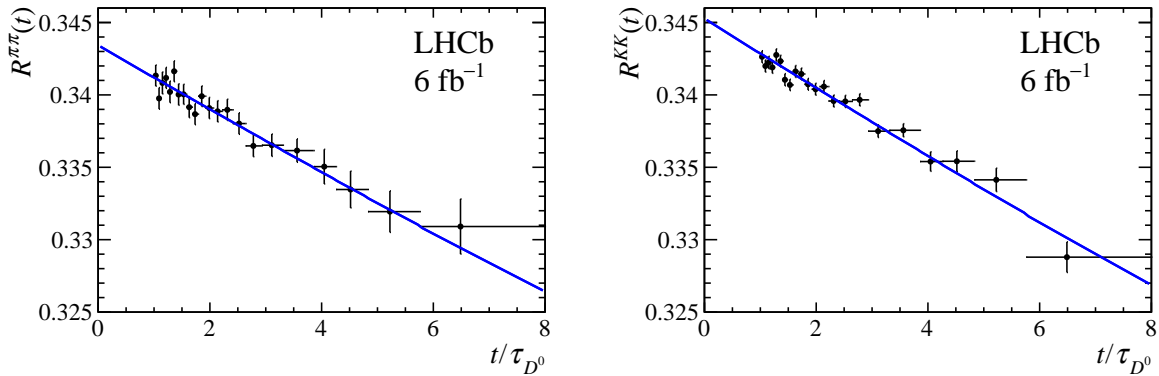
Figure 7: Distributions of (left) $R^{\pi\pi}(t)$ and (right) $R^{KK}(t)$ using the full LHCb Run 2 data set, with the results of $y_{CP}^{\pi\pi} - y_{CP}^{K\pi}$ and $y_{CP}^{KK} - y_{CP}^{K\pi}$ overlaid as the blue slopes.

The background fraction is measured to be 11.8×10^{-4}. Using the RapidSim samples, the impact of these contributions on the measurements of $y_{CP}^{\pi\pi} - y_{CP}^{K\pi}$ and $y_{CP}^{KK} - y_{CP}^{K\pi}$ is evaluated to be 0.02×10^{-3} and 0.11×10^{-3}, respectively. These values are assigned as systematic uncertainties.

A third source of systematic uncertainty arises from the precision on the determination of the time-dependent fraction of secondary decays $f_{\rm sec}(t)$, and the average true D^0 decay time $\langle t_D \rangle$ as a function of the reconstructed D^0 decay time t. The uncertainty in the determination of $f_{\rm sec}(t)$ receives three separate contributions. First, in the fits to IP(D^0), discrepancies in the ratio between the fit model and data are seen to reach up to 10%. The impact of these discrepancies to the measurement is assigned as a systematic uncertainty. Second, the fits to IP(D^0) are performed in the interval $[0, 200]\,\mu$m. The impact of increasing the upper bound of the interval to $600\,\mu$m results in a small variation to the $y_{CP}^{f} - y_{CP}^{K\pi}$ measurements, which is assigned as a systematic uncertainty. Finally, the simulation samples of prompt and secondary candidates are produced for the 2017 and 2018 data conditions only, and a systematic uncertainty is assigned by considering the impact to the measurement of potential variations to the distribution of IP(D^0) in the 2015 and 2016 data taking conditions. The uncertainty in the determination of $\langle t_D(t) \rangle$ receives two independent contributions. First, the impact on the difference of lifetimes between B^0 and B^+ mesons is considered by determining $\langle t_D \rangle(t)$ using simulation samples of alternatively only B^0 or B^+ candidates. Then, the effect of the weighting of the simulation samples is evaluated by determining $\langle t_D(t) \rangle$ with and without the weighting. The total systematic uncertainty related to the treatment of secondary decays is evaluated to be at the level of 0.03×10^{-3} for both the $y_{CP}^{\pi\pi} - y_{CP}^{K\pi}$ and the $y_{CP}^{KK} - y_{CP}^{K\pi}$ measurements.

A systematic uncertainty related to the kinematic weighting procedure is assigned by using alternative input variables and particles of the decay chain to the weighting algorithm and repeating the measurement. An additional systematic uncertainty is assigned by performing the weighting of the target decay to the matched one. The systematic uncertainties are summed in quadrature and determined as 0.08×10^{-3} for $y_{CP}^{\pi\pi} - y_{CP}^{K\pi}$ and 0.02×10^{-3} for $y_{CP}^{KK} - y_{CP}^{K\pi}$.

The uncertainty on the current world average value of the lifetime of the D^0 meson [1] is propagated as a systematic uncertainty and is estimated as 0.03×10^{-3} for both measurements.

14

Table 2: Systematic uncertainties for the $y_{CP}^{\pi\pi} - y_{CP}^{K\pi}$ and $y_{CP}^{KK} - y_{CP}^{K\pi}$ measurements.

	$\sigma(y_{CP}^{\pi\pi} - y_{CP}^{K\pi})$ [10^{-3}]	$\sigma(y_{CP}^{KK} - y_{CP}^{K\pi})$ [10^{-3}]
Combinatorial background	0.12	0.07
Peaking background	0.02	0.11
Treatment of secondary decays	0.03	0.03
Kinematic weighting procedure	0.08	0.02
Input D^0 lifetime	0.03	0.03
Residual nuisance asymmetries	0.03	< 0.01
Fit bias	0.03	0.03
Total	0.16	0.14

A source of systematic uncertainty includes a potential bias related to the contributions from the flavour of the D^0 meson, which can arise from tagging-pion detection asymmetries and D^{*+} production asymmetries. The size of such a bias is estimated by performing the measurement separating the two D^0 flavours. The D^0 and $\overline{D}^0$ measurements are seen to be compatible within the 1σ level. The weighted average of the D^0 and $\overline{D}^0$ measurements is compared to the baseline measurement where both D^0 and $\overline{D}^0$ samples are merged. For $y_{CP}^{\pi\pi} - y_{CP}^{K\pi}$, the difference between the two strategies is measured as 0.03×10^{-3}, while for $y_{CP}^{KK} - y_{CP}^{K\pi}$ it is found to be below 0.01×10^{-3}. These values are assigned as systematic uncertainty.

It is suggested in Ref. [13] that in the expansion of $R^f(t)$, the second-order terms of the decay time and mixing parameters differ from those of the exponential function used in the baseline fit. To estimate potential resulting biases, one thousand pseudoexperiments consisting of samples of Cabibbo-suppressed and Cabibbo-favoured decays are generated according to the theoretical model described in Ref. [13], using the current world average values of charm mixing and CP-violation parameters [11]. For each pseudoexperiment, $R^f(t)$ is fitted with an exponential function and the departure of the mean value of the fits from the expectation of the theoretical model is measured as 0.03×10^{-3}, and is assigned as a systematic uncertainty. The summary of the systematic uncertainties is presented in Table 2, where the quadratic sum of all contributions is 0.16×10^{-3} for $y_{CP}^{\pi\pi} - y_{CP}^{K\pi}$ and 0.14×10^{-3} for $y_{CP}^{KK} - y_{CP}^{K\pi}$.

Robustness checks are performed by verifying that the measurements do not show any dependence on various variables, including the momentum, transverse momentum, the pseudorapidity and azimuthal angle of the D^0 and π_{tag}^+ mesons, as well as the D^0 flight distance in the plane transverse to the beam and the z coordinate of the D^0 decay vertex. No significant dependence of $y_{CP}^f - y_{CP}^{K\pi}$ on any of the listed variables is observed. To study a potential dependence on the orientation of the magnetic field and on a potential left-right asymmetry of the detector, the measurement is performed separately for positive and negative values of the x component of the momentum of the D^0 meson, and for the *MagUp* and *MagDown* polarities. All measurements are seen to be statistically compatible within two standard deviations. To evaluate the impact of possible residual resolution effects at low values of D^0 decay time, the measurements of $y_{CP}^f - y_{CP}^{K\pi}$ are performed by

increasing successively the lower window of the D^0 decay time up to $1.7\,\tau_{D^0}$. Accounting for the statistical overlap, all measured values are found to be statistically compatible and correspondingly no systematic uncertainty is assigned to this effect.

Due to the presence of correlations between the reconstructed D^0 decay time and momentum, the correction procedure can introduce a bias to the true values of $y_{CP}^{f} - y_{CP}^{K\pi}$. To study this bias, artificial values of $y_{CP}^{f} - y_{CP}^{K\pi}$ are injected to the data samples by altering the decay time distribution of numerator decays. Both kinematic matching and weighting procedures are applied and the measured values are compared to the injected ones. The procedure is performed for ten values in the interval $[-25, 25] \times 10^{-3}$. The measured and injected values agree, confirming that no significant bias is seen and correspondingly no systematic uncertainty is applied.

9   Summary and conclusion

The measurements of the ratios of the effective decay widths of $D^0 \to \pi^- \pi^+$ and $D^0 \to K^- K^+$ decays over that of $D^0 \to K^- \pi^+$ decays are performed with the LHCb experiment using pp collisions at a centre-of-mass energy of $13\,\text{TeV}$, corresponding to an integrated luminosity of $6\,\text{fb}^{-1}$. The ratios give direct access to the charm mixing parameters $y_{CP}^{\pi\pi} - y_{CP}^{K\pi}$ and $y_{CP}^{KK} - y_{CP}^{K\pi}$, which are measured to be

$$y_{CP}^{\pi\pi} - y_{CP}^{K\pi} = (6.57 \pm 0.53 \pm 0.16) \times 10^{-3},$$
$$y_{CP}^{KK} - y_{CP}^{K\pi} = (7.08 \pm 0.30 \pm 0.14) \times 10^{-3},$$

where the first uncertainties are statistical and the second systematic. Assuming that all systematic uncertainties are fully correlated, except those of the peaking background contributions which are considered as uncorrelated, the combination of the two measurements yields

$$y_{CP} - y_{CP}^{K\pi} = (6.96 \pm 0.26 \pm 0.13) \times 10^{-3}.$$

This result is compatible with the present world average [16] and more precise by a factor of four.

A combination of LHCb charm measurements is performed using the statistical framework detailed in Ref. [11]. When the present result is added, the mixing parameter y is found to be equal to $y = \left(6.46 \pm^{+0.24}_{-0.25}\right) \times 10^{-3}$, improving its current sensitivity by more than a factor of two [16]. In addition, the strong phase difference between the $D^0 \to K^\mp \pi^\pm$ decay amplitudes is $\delta_{K\pi} = \left(192.1^{+3.7}_{-4.0}\right)^\circ$ and departs from 180° by about three standard deviations, indicating an evidence for U-spin symmetry breaking.

The precision on y and $\delta_{K\pi}$ can be further reduced by a simultaneous combination of charm results with measurements of the Cabibbo-Kobayashi-Maskawa angle γ in beauty decays, as first done in Ref. [11]. This will be the subject of a separate publication.

Acknowledgements

References

[1] Particle Data Group, P. A. Zyla *et al.*, *Review of particle physics*, Prog. Theor. Exp. Phys. **2020** (2020) 083C01.

[2] Y. Grossman, Y. Nir, and G. Perez, *Testing new indirect CP violation*, Phys. Rev. Lett. **103** (2009) 071602, `arXiv:0904.0305`.

[3] A. L. Kagan and M. D. Sokoloff, *Indirect CP violation and implications for $D^0 - \overline{D}^0$ and $B^0_s - \overline{B}^0_s$ mixing*, Phys. Rev. **D80** (2009) 076008, `arXiv:0907.3917`.

[4] BaBar collaboration, P. del Amo Sanchez *et al.*, *Measurement of D^0–$\overline{D}^0$ mixing parameters using $D^0 \to K^0_S \pi^+ \pi^-$ and $D^0 \to K^0_S K^+ K^-$ decays*, Phys. Rev. Lett. **105** (2010) 081803, `arXiv:1004.5053`.

[5] BaBar collaboration, J. P. Lees *et al.*, *Measurement of D^0–$\overline{D}^0$ mixing and CP violation in two-body D^0 decays*, Phys. Rev. **D87** (2013) 012004, `arXiv:1209.3896`.

[6] Belle collaboration, T. Peng *et al.*, *Measurement of D^0–$\overline{D}^0$ mixing and search for indirect CP violation using $D^0 \to K^0_S \pi^+ \pi^-$ decays*, Phys. Rev. **D89** (2014) 091103, `arXiv:1404.2412`.

[7] Belle collaboration, M. Starič *et al.*, *Measurement of D^0–$\overline{D}^0$ mixing and search for CP violation in $D^0 \to K^+ K^-, \pi^+ \pi^-$ decays with the full Belle data set*, Phys. Lett. **B753** (2016) 412, `arXiv:1509.08266`.

[8] LHCb collaboration, R. Aaij *et al.*, *Updated determination of D^0–$\overline{D}^0$ mixing and CP violation parameters with $D^0 \to K^+ \pi^-$ decays*, Phys. Rev. **D97** (2018) 031101, `arXiv:1712.03220`.

[9] LHCb collaboration, R. Aaij *et al.*, *Measurement of the charm-mixing parameter y_{CP}*, Phys. Rev. Lett. **122** (2019) 011802, `arXiv:1810.06874`.

[10] LHCb collaboration, R. Aaij *et al.*, *Observation of the mass difference between neutral charm-meson eigenstates*, Phys. Rev. Lett. **127** (2021) 111801, `arXiv:2106.03744`.

[11] LHCb collaboration, R. Aaij *et al.*, *Simultaneous determination of CKM angle γ and charm mixing parameters*, JHEP **12** (2021) 141, `arXiv:2110.02350`.

[12] A. L. Kagan and L. Silvestrini, *Dispersive and absorptive CP violation in $D^0 - \overline{D^0}$ mixing*, Phys. Rev. **D103** (2021) 053008, `arXiv:2001.07207`.

[13] T. Pajero and M. J. Morello, *Mixing and CP violation in $D^0 \to K^- \pi^+$ decays*, JHEP **03** (2022) 162, `arXiv:2106.02014`.

[14] T. Pajero, *CharmFitter*, `https://github.com/tpajero/charm-fitter/`.

[15] LHCb collaboration, R. Aaij *et al.*, *Measurement of mixing and CP violation parameters in two-body charm decays*, JHEP **04** (2012) 129, `arXiv:1112.4698`.

[16] Heavy Flavor Averaging Group, Y. Amhis *et al.*, *Averages of b-hadron, c-hadron, and τ-lepton properties as of 2018*, Eur. Phys. J. **C81** (2021) 226, arXiv:1909.12524, updated results and plots available at https://hflav.web.cern.ch.

[17] LHCb collaboration, A. A. Alves Jr. *et al.*, *The LHCb detector at the LHC*, JINST **3** (2008) S08005.

[18] LHCb collaboration, R. Aaij *et al.*, *LHCb detector performance*, Int. J. Mod. Phys. **A30** (2015) 1530022, arXiv:1412.6352.

[19] R. Aaij *et al.*, *The LHCb trigger and its performance in 2011*, JINST **8** (2013) P04022, arXiv:1211.3055.

[20] R. Aaij *et al.*, *Tesla: an application for real-time data analysis in High Energy Physics*, Comput. Phys. Commun. **208** (2016) 35, arXiv:1604.05596.

[21] T. Sjöstrand, S. Mrenna, and P. Skands, *A brief introduction to PYTHIA 8.1*, Comput. Phys. Commun. **178** (2008) 852, arXiv:0710.3820.

[22] I. Belyaev *et al.*, *Handling of the generation of primary events in Gauss, the LHCb simulation framework*, J. Phys. Conf. Ser. **331** (2011) 032047.

[23] Geant4 collaboration, J. Allison *et al.*, *Geant4 developments and applications*, IEEE Trans. Nucl. Sci. **53** (2006) 270.

[24] M. Clemencic *et al.*, *The LHCb simulation application, Gauss: Design, evolution and experience*, J. Phys. Conf. Ser. **331** (2011) 032023.

[25] D. J. Lange, *The EvtGen particle decay simulation package*, Nucl. Instrum. Meth. **A462** (2001) 152.

[26] E. Barberio, B. van Eijk, and Z. Was, *Photos — a universal Monte Carlo for QED radiative corrections in decays*, Computer Physics Communications **66** (1991) 115.

[27] G. A. Cowan, D. C. Craik, and M. D. Needham, *RapidSim: an application for the fast simulation of heavy-quark hadron decays*, Comput. Phys. Commun. **214** (2017) 239, arXiv:1612.07489.

[28] G. Pietrzyk, *Precision measurement of neutral charm meson mixing parameters*, PhD thesis, École Polytechnique fédérale de Lausanne (EPFL), 2021, CERN-THESIS-2021-295.

[29] A. Rogozhnikov *et al.*, *hep ml - machine learning algorithms for high energy physics*, https://arogozhnikov.github.io/hep_ml/.

[30] V. V. Gligorov and M. W. Kenzie, *Lifetime unbiased beauty and charm triggers at LHCb*, LHCb-PUB-2015-026, 2016.

[31] W. D. Hulsbergen, *Decay chain fitting with a Kalman filter*, Nucl. Instrum. Meth. **A552** (2005) 566, arXiv:physics/0503191.

[32] R. Aaij *et al.*, *Performance of the LHCb Vertex Locator*, JINST **9** (2014) P09007, arXiv:1405.7808.

[33] N. L. Johnson, *Systems of frequency curves generated by methods of translation*, Biometrika **36** (1949) 149.

LHCb collaboration

R. Aaij[32], A.S.W. Abdelmotteleb[56], C. Abellán Beteta[50], F. Abudinén[56], T. Ackernley[60],
B. Adeva[46], M. Adinolfi[54], H. Afsharnia[9], C. Agapopoulou[13], C.A. Aidala[87], S. Aiola[25],
Z. Ajaltouni[9], S. Akar[65], J. Albrecht[15], F. Alessio[48], M. Alexander[59], A. Alfonso Albero[45],
Z. Aliouche[62], G. Alkhazov[38], P. Alvarez Cartelle[55], S. Amato[2], J.L. Amey[54], Y. Amhis[11],
L. An[48], L. Anderlini[22], M. Andersson[50], A. Andreianov[38], M. Andreotti[21], D. Ao[6],
F. Archilli[17], A. Artamonov[44], M. Artuso[68], K. Arzymatov[42], E. Aslanides[10], M. Atzeni[50],
B. Audurier[12], S. Bachmann[17], M. Bachmayer[49], J.J. Back[56], P. Baladron Rodriguez[46],
V. Balagura[12], W. Baldini[21], J. Baptista de Souza Leite[1], M. Barbetti[22,h], R.J. Barlow[62],
S. Barsuk[11], W. Barter[61], M. Bartolini[55], F. Baryshnikov[83], J.M. Basels[14], G. Bassi[29],
B. Batsukh[4], A. Battig[15], A. Bay[49], A. Beck[56], M. Becker[15], F. Bedeschi[29], I. Bediaga[1],
A. Beiter[68], V. Belavin[42], S. Belin[46], V. Bellee[50], K. Belous[44], I. Belov[40], I. Belyaev[41],
G. Bencivenni[23], E. Ben-Haim[13], A. Berezhnoy[40], R. Bernet[50], D. Berninghoff[17],
H.C. Bernstein[68], C. Bertella[62], A. Bertolin[28], C. Betancourt[50], F. Betti[48], Ia. Bezshyiko[50],
S. Bhasin[54], J. Bhom[35], L. Bian[73], M.S. Bieker[15], N.V. Biesuz[21], S. Bifani[53], P. Billoir[13],
A. Biolchini[32], M. Birch[61], F.C.R. Bishop[55], A. Bitadze[62], A. Bizzeti[22,l], M. Bjørn[63],
M.P. Blago[55], T. Blake[56], F. Blanc[49], S. Blusk[68], D. Bobulska[59], J.A. Boelhauve[15],
O. Boente Garcia[46], T. Boettcher[65], A. Boldyrev[82], A. Bondar[43], N. Bondar[38,48], S. Borghi[62],
M. Borisyak[42], M. Borsato[17], J.T. Borsuk[35], S.A. Bouchiba[49], T.J.V. Bowcock[60,48], A. Boyer[48],
C. Bozzi[21], M.J. Bradley[61], S. Braun[66], A. Brea Rodriguez[46], J. Brodzicka[35],
A. Brossa Gonzalo[56], D. Brundu[27], A. Buonaura[50], L. Buonincontri[28], A.T. Burke[62], C. Burr[48],
A. Bursche[72], A. Butkevich[39], J.S. Butter[32], J. Buytaert[48], W. Byczynski[48], S. Cadeddu[27],
H. Cai[73], R. Calabrese[21,g], L. Calefice[15,13], S. Cali[23], R. Calladine[53], M. Calvi[26,k],
M. Calvo Gomez[85], P. Camargo Magalhaes[54], P. Campana[23], A.F. Campoverde Quezada[6],
S. Capelli[26,k], L. Capriotti[20,e], A. Carbone[20,e], G. Carboni[31,q], R. Cardinale[24,i], A. Cardini[27],
I. Carli[4], P. Carniti[26,k], L. Carus[14], K. Carvalho Akiba[32], A. Casais Vidal[46], R. Caspary[17],
G. Casse[60], M. Cattaneo[48], G. Cavallero[48], S. Celani[49], J. Cerasoli[10], D. Cervenkov[63],
A.J. Chadwick[60], M.G. Chapman[54], M. Charles[13], Ph. Charpentier[48], C.A. Chavez Barajas[60],
M. Chefdeville[8], C. Chen[3], S. Chen[4], A. Chernov[35], V. Chobanova[46], S. Cholak[49],
M. Chrzaszcz[35], A. Chubykin[38], V. Chulikov[38], P. Ciambrone[23], M.F. Cicala[56], X. Cid Vidal[46],
G. Ciezarek[48], P.E.L. Clarke[58], M. Clemencic[48], H.V. Cliff[55], J. Closier[48], J.L. Cobbledick[62],
V. Coco[48], J.A.B. Coelho[11], J. Cogan[10], E. Cogneras[9], L. Cojocariu[37], P. Collins[48],
T. Colombo[48], L. Congedo[19,d], A. Contu[27], N. Cooke[53], G. Coombs[59], I. Corredoira [46],
G. Corti[48], C.M. Costa Sobral[56], B. Couturier[48], D.C. Craik[64], J. Crkovská[67], M. Cruz Torres[1],
R. Currie[58], C.L. Da Silva[67], S. Dadabaev[83], L. Dai[71], E. Dall'Occo[15], J. Dalseno[46],
C. D'Ambrosio[48], A. Danilina[41], P. d'Argent[48], A. Dashkina[83], J.E. Davies[62], A. Davis[62],
O. De Aguiar Francisco[62], K. De Bruyn[79], S. De Capua[62], M. De Cian[49],
U. De Freitas Carneiro Da Graca[1], E. De Lucia[23], J.M. De Miranda[1], L. De Paula[2],
M. De Serio[19,d], D. De Simone[50], P. De Simone[23], F. De Vellis[15], J.A. de Vries[80], C.T. Dean[67],
F. Debernardis[19,d], D. Decamp[8], V. Dedu[10], L. Del Buono[13], B. Delaney[55], H.-P. Dembinski[15],
V. Denysenko[50], D. Derkach[82], O. Deschamps[9], F. Dettori[27,f], B. Dey[77], A. Di Cicco[23],
P. Di Nezza[23], S. Didenko[83], L. Dieste Maronas[46], S. Ding[68], V. Dobishuk[52], C. Dong[3],
A.M. Donohoe[18], F. Dordei[27], A.C. dos Reis[1], L. Douglas[59], A. Dovbnya[51], A.G. Downes[8],
M.W. Dudek[35], L. Dufour[48], V. Duk[78], P. Durante[48], J.M. Durham[67], D. Dutta[62], A. Dziurda[35],
A. Dzyuba[38], S. Easo[57], U. Egede[69], V. Egorychev[41], S. Eidelman[43,u,†], S. Eisenhardt[58],
S. Ek-In[49], L. Eklund[86], S. Ely[68], A. Ene[37], E. Epple[67], S. Escher[14], J. Eschle[50], S. Esen[50],
T. Evans[62], L.N. Falcao[1], Y. Fan[6], B. Fang[73], S. Farry[60], D. Fazzini[26,k], M. Féo[48],
A. Fernandez Prieto[46], A.D. Fernez[66], F. Ferrari[20], L. Ferreira Lopes[49], F. Ferreira Rodrigues[2],
S. Ferreres Sole[32], M. Ferrillo[50], M. Ferro-Luzzi[48], S. Filippov[39], R.A. Fini[19], M. Fiorini[21,g],

M. Firlej[34], K.M. Fischer[63], D.S. Fitzgerald[87], C. Fitzpatrick[62], T. Fiutowski[34], A. Fkiaras[48],
F. Fleuret[12], M. Fontana[13], F. Fontanelli[24,i], R. Forty[48], D. Foulds-Holt[55], V. Franco Lima[60],
M. Franco Sevilla[66], M. Frank[48], E. Franzoso[21], G. Frau[17], C. Frei[48], D.A. Friday[59], J. Fu[6],
Q. Fuehring[15], E. Gabriel[32], G. Galati[19,d], A. Gallas Torreira[46], D. Galli[20,e], S. Gambetta[58,48],
Y. Gan[3], M. Gandelman[2], P. Gandini[25], Y. Gao[5], M. Garau[27], L.M. Garcia Martin[56],
P. Garcia Moreno[45], J. García Pardiñas[26,k], B. Garcia Plana[46], F.A. Garcia Rosales[12],
L. Garrido[45], C. Gaspar[48], R.E. Geertsema[32], D. Gerick[17], L.L. Gerken[15], E. Gersabeck[62],
M. Gersabeck[62], T. Gershon[56], L. Giambastiani[28], V. Gibson[55], H.K. Giemza[36], A.L. Gilman[63],
M. Giovannetti[23,q], A. Gioventù[46], P. Gironella Gironell[45], C. Giugliano[21], K. Gizdov[58],
E.L. Gkougkousis[48], V.V. Gligorov[13,48], C. Göbel[70], E. Golobardes[85], D. Golubkov[41],
A. Golutvin[61,83], A. Gomes[1,a], S. Gomez Fernandez[45], F. Goncalves Abrantes[63], M. Goncerz[35],
G. Gong[3], P. Gorbounov[41], I.V. Gorelov[40], C. Gotti[26], J.P. Grabowski[17], T. Grammatico[13],
L.A. Granado Cardoso[48], E. Graugés[45], E. Graverini[49], G. Graziani[22], A. Grecu[37],
L.M. Greeven[32], N.A. Grieser[4], L. Grillo[62], S. Gromov[83], B.R. Gruberg Cazon[63], C. Gu[3],
M. Guarise[21], M. Guittiere[11], P. A. Günther[17], E. Gushchin[39], A. Guth[14], Y. Guz[44], T. Gys[48],
T. Hadavizadeh[69], G. Haefeli[49], C. Haen[48], J. Haimberger[48], S.C. Haines[55],
T. Halewood-leagas[60], P.M. Hamilton[66], J.P. Hammerich[60], Q. Han[7], X. Han[17], E.B. Hansen[62],
S. Hansmann-Menzemer[17,48], N. Harnew[63], T. Harrison[60], C. Hasse[48], M. Hatch[48], J. He[6,b],
K. Heijhoff[32], K. Heinicke[15], R.D.L. Henderson[69,56], A.M. Hennequin[64], K. Hennessy[60],
L. Henry[48], J. Heuel[14], A. Hicheur[2], D. Hill[49], M. Hilton[62], S.E. Hollitt[15], R. Hou[7], Y. Hou[8],
J. Hu[17], J. Hu[72], W. Hu[7], X. Hu[3], W. Huang[6], X. Huang[73], W. Hulsbergen[32], R.J. Hunter[56],
M. Hushchyn[82], D. Hutchcroft[60], D. Hynds[32], P. Ibis[15], M. Idzik[34], D. Ilin[38], P. Ilten[65],
A. Inglessi[38], A. Iniukhin[82], A. Ishteev[83], K. Ivshin[38], R. Jacobsson[48], H. Jage[14], S. Jakobsen[48],
E. Jans[32], B.K. Jashal[47], A. Jawahery[66], V. Jevtic[15], X. Jiang[4], M. John[63], D. Johnson[64],
C.R. Jones[55], T.P. Jones[56], B. Jost[48], N. Jurik[48], S. Kandybei[51], Y. Kang[3], M. Karacson[48],
D. Karpenkov[83], M. Karpov[82], J.W. Kautz[65], F. Keizer[48], D.M. Keller[68], M. Kenzie[56],
T. Ketel[33], B. Khanji[15], A. Kharisova[84], S. Kholodenko[44,83], T. Kirn[14], V.S. Kirsebom[49],
O. Kitouni[64], S. Klaver[33], N. Kleijne[29], K. Klimaszewski[36], M.R. Kmiec[36], S. Koliiev[52],
A. Kondybayeva[83], A. Konoplyannikov[41], P. Kopciewicz[34], R. Kopecna[17], P. Koppenburg[32],
M. Korolev[40], I. Kostiuk[32,52], O. Kot[52], S. Kotriakhova[21,38], A. Kozachuk[40], P. Kravchenko[38],
L. Kravchuk[39], R.D. Krawczyk[48], M. Kreps[56], S. Kretzschmar[14], P. Krokovny[43,u], W. Krupa[34],
W. Krzemien[36], J. Kubat[17], M. Kucharczyk[35], V. Kudryavtsev[43,u], H.S. Kuindersma[32,33],
G.J. Kunde[67], T. Kvaratskheliya[41], D. Lacarrere[48], G. Lafferty[62], A. Lai[27], A. Lampis[27],
D. Lancierini[50], J.J. Lane[62], R. Lane[54], G. Lanfranchi[23], C. Langenbruch[14], J. Langer[15],
O. Lantwin[83], T. Latham[56], F. Lazzari[29], R. Le Gac[10], S.H. Lee[87], R. Lefèvre[9], A. Leflat[40],
S. Legotin[83], O. Leroy[10], T. Lesiak[35], B. Leverington[17], H. Li[72], P. Li[17], S. Li[7], Y. Li[4], Z. Li[68],
X. Liang[68], T. Lin[57], R. Lindner[48], V. Lisovskyi[15], R. Litvinov[27], G. Liu[72], H. Liu[6], Q. Liu[6],
S. Liu[4], A. Lobo Salvia[45], A. Loi[27], R. Lollini[78], J. Lomba Castro[46], I. Longstaff[59], J.H. Lopes[2],
S. López Soliño[46], G.H. Lovell[55], Y. Lu[4], C. Lucarelli[22,h], D. Lucchesi[28,m], S. Luchuk[39],
M. Lucio Martinez[32], V. Lukashenko[32,52], Y. Luo[3], A. Lupato[62], E. Luppi[21,g], O. Lupton[56],
A. Lusiani[29,n], X. Lyu[6], L. Ma[4], R. Ma[6], S. Maccolini[20], F. Machefert[11], F. Maciuc[37],
V. Macko[49], P. Mackowiak[15], S. Maddrell-Mander[54], L.R. Madhan Mohan[54], O. Maev[38],
A. Maevskiy[82], D. Maisuzenko[38], M.W. Majewski[34], J.J. Malczewski[35], S. Malde[63],
B. Malecki[35], A. Malinin[81], T. Maltsev[43,u], H. Malygina[17], G. Manca[27,f], G. Mancinelli[10],
D. Manuzzi[20], C.A. Manzari[50], D. Marangotto[25,j], J. Maratas[9,s], J.F. Marchand[8], U. Marconi[20],
S. Mariani[22,h], C. Marin Benito[48], M. Marinangeli[49], J. Marks[17], A.M. Marshall[54],
P.J. Marshall[60], G. Martelli[78], G. Martellotti[30], L. Martinazzoli[48,k], M. Martinelli[26,k],
D. Martinez Santos[46], F. Martinez Vidal[47], A. Massafferri[1], M. Materok[14], R. Matev[48],
A. Mathad[50], V. Matiunin[41], C. Matteuzzi[26], K.R. Mattioli[87], A. Mauri[32], E. Maurice[12],
J. Mauricio[45], M. Mazurek[48], M. McCann[61], L. Mcconnell[18], T.H. Mcgrath[62], N.T. Mchugh[59],

A. McNab[62], R. McNulty[18], J.V. Mead[60], B. Meadows[65], G. Meier[15], D. Melnychuk[36],
S. Meloni[26,k], M. Merk[32,80], A. Merli[25,j], L. Meyer Garcia[2], M. Mikhasenko[75,c], D.A. Milanes[74],
E. Millard[56], M. Milovanovic[48], M.-N. Minard[8], A. Minotti[26,k], S.E. Mitchell[58], B. Mitreska[62],
D.S. Mitzel[15], A. Mödden [15], R.A. Mohammed[63], R.D. Moise[61], S. Mokhnenko[82],
T. Mombächer[46], I.A. Monroy[74], S. Monteil[9], M. Morandin[28], G. Morello[23], M.J. Morello[29,n],
J. Moron[34], A.B. Morris[75], A.G. Morris[56], R. Mountain[68], H. Mu[3], F. Muheim[58], M. Mulder[79],
K. Müller[50], C.H. Murphy[63], D. Murray[62], R. Murta[61], P. Muzzetto[27], P. Naik[54], T. Nakada[49],
R. Nandakumar[57], T. Nanut[48], I. Nasteva[2], M. Needham[58], N. Neri[25,j], S. Neubert[75],
N. Neufeld[48], R. Newcombe[61], E.M. Niel[49], S. Nieswand[14], N. Nikitin[40], N.S. Nolte[64],
C. Normand[8], C. Nunez[87], A. Oblakowska-Mucha[34], V. Obraztsov[44], T. Oeser[14],
D.P. O'Hanlon[54], S. Okamura[21], R. Oldeman[27,f], F. Oliva[58], M.E. Olivares[68],
C.J.G. Onderwater[79], R.H. O'Neil[58], J.M. Otalora Goicochea[2], T. Ovsiannikova[41], P. Owen[50],
A. Oyanguren[47], O. Ozcelik[58], K.O. Padeken[75], B. Pagare[56], P.R. Pais[48], T. Pajero[63],
A. Palano[19], M. Palutan[23], Y. Pan[62], G. Panshin[84], A. Papanestis[57], M. Pappagallo[19,d],
L.L. Pappalardo[21], C. Pappenheimer[65], W. Parker[66], C. Parkes[62], B. Passalacqua[21],
G. Passaleva[22], A. Pastore[19], M. Patel[61], C. Patrignani[20,e], C.J. Pawley[80], A. Pearce[48,57],
A. Pellegrino[32], M. Pepe Altarelli[48], S. Perazzini[20], D. Pereima[41], A. Pereiro Castro[46],
P. Perret[9], M. Petric[59,48], K. Petridis[54], A. Petrolini[24,i], A. Petrov[81], S. Petrucci[58],
M. Petruzzo[25], T.T.H. Pham[68], A. Philippov[42], R. Piandani[6], L. Pica[29,n], M. Piccini[78],
B. Pietrzyk[8], G. Pietrzyk[11], M. Pili[63], D. Pinci[30], F. Pisani[48], M. Pizzichemi[26,48,k], Resmi
P.K[10], V. Placinta[37], J. Plews[53], M. Plo Casasus[46], F. Polci[13,48], M. Poli Lener[23],
M. Poliakova[68], A. Poluektov[10], N. Polukhina[83,t], I. Polyakov[68], E. Polycarpo[2], S. Ponce[48],
D. Popov[6,48], S. Popov[42], S. Poslavskii[44], K. Prasanth[35], L. Promberger[48], C. Prouve[46],
V. Pugatch[52], V. Puill[11], G. Punzi[29,o], H. Qi[3], W. Qian[6], N. Qin[3], R. Quagliani[49], N.V. Raab[18],
R.I. Rabadan Trejo[6], B. Rachwal[34], J.H. Rademacker[54], R. Rajagopalan[68], M. Rama[29],
M. Ramos Pernas[56], M.S. Rangel[2], F. Ratnikov[42,82], G. Raven[33,48], M. Reboud[8], F. Redi[48],
F. Reiss[62], C. Remon Alepuz[47], Z. Ren[3], V. Renaudin[63], R. Ribatti[29], A.M. Ricci[27],
S. Ricciardi[57], K. Rinnert[60], P. Robbe[11], G. Robertson[58], A.B. Rodrigues[49], E. Rodrigues[60],
J.A. Rodriguez Lopez[74], E.R.R. Rodriguez Rodriguez[46], A. Rollings[63], P. Roloff[48],
V. Romanovskiy[44], M. Romero Lamas[46], A. Romero Vidal[46], J.D. Roth[87], M. Rotondo[23],
M.S. Rudolph[68], T. Ruf[48], R.A. Ruiz Fernandez[46], J. Ruiz Vidal[47], A. Ryzhikov[82], J. Ryzka[34],
J.J. Saborido Silva[46], N. Sagidova[38], N. Sahoo[53], B. Saitta[27,f], M. Salomoni[48],
C. Sanchez Gras[32], I. Sanderswood[47], R. Santacesaria[30], C. Santamarina Rios[46],
M. Santimaria[23], E. Santovetti[31,q], D. Saranin[83], G. Sarpis[14], M. Sarpis[75], A. Sarti[30],
C. Satriano[30,p], A. Satta[31], M. Saur[15], D. Savrina[41,40], H. Sazak[9], L.G. Scantlebury Smead[63],
A. Scarabotto[13], S. Schael[14], S. Scherl[60], M. Schiller[59], H. Schindler[48], M. Schmelling[16],
B. Schmidt[48], S. Schmitt[14], O. Schneider[49], A. Schopper[48], M. Schubiger[32], S. Schulte[49],
M.H. Schune[11], R. Schwemmer[48], B. Sciascia[23,48], S. Sellam[46], A. Semennikov[41],
M. Senghi Soares[33], A. Sergi[24,i], N. Serra[50], L. Sestini[28], A. Seuthe[15], Y. Shang[5],
D.M. Shangase[87], M. Shapkin[44], I. Shchemerov[83], L. Shchutska[49], T. Shears[60],
L. Shekhtman[43,u], Z. Shen[5], S. Sheng[4], V. Shevchenko[81], E.B. Shields[26,k], Y. Shimizu[11],
E. Shmanin[83], J.D. Shupperd[68], B.G. Siddi[21], R. Silva Coutinho[50], G. Simi[28], S. Simone[19,d],
M. Singla[69], N. Skidmore[62], R. Skuza[17], T. Skwarnicki[68], M.W. Slater[53], I. Slazyk[21,g],
J.C. Smallwood[63], J.G. Smeaton[55], E. Smith[50], M. Smith[61], A. Snoch[32], L. Soares Lavra[9],
M.D. Sokoloff[65], F.J.P. Soler[59], A. Solovev[38], I. Solovyev[38], F.L. Souza De Almeida[2],
B. Souza De Paula[2], B. Spaan[15], E. Spadaro Norella[25,j], P. Spradlin[59], F. Stagni[48], M. Stahl[65],
S. Stahl[48], S. Stanislaus[63], O. Steinkamp[50,83], O. Stenyakin[44], H. Stevens[15], S. Stone[68,48,†],
D. Strekalina[83], F. Suljik[63], J. Sun[27], L. Sun[73], Y. Sun[66], P. Svihra[62], P.N. Swallow[53],
K. Swientek[34], A. Szabelski[36], T. Szumlak[34], M. Szymanski[48], S. Taneja[62], A.R. Tanner[54],
M.D. Tat[63], A. Terentev[83], F. Teubert[48], E. Thomas[48], D.J.D. Thompson[53], K.A. Thomson[60],

23

H. Tilquin[61], V. Tisserand[9], S. T'Jampens[8], M. Tobin[4], L. Tomassetti[21,g], X. Tong[5],
D. Torres Machado[1], D.Y. Tou[3], E. Trifonova[83], S.M. Trilov[54], C. Trippl[49], G. Tuci[6], A. Tully[49],
N. Tuning[32,48], A. Ukleja[36], D.J. Unverzagt[17], E. Ursov[83], A. Usachov[32], A. Ustyuzhanin[42,82],
U. Uwer[17], A. Vagner[84], V. Vagnoni[20], A. Valassi[48], G. Valenti[20], N. Valls Canudas[85],
M. van Beuzekom[32], M. Van Dijk[49], H. Van Hecke[67], E. van Herwijnen[83], M. van Veghel[79],
R. Vazquez Gomez[45], P. Vazquez Regueiro[46], C. Vázquez Sierra[48], S. Vecchi[21], J.J. Velthuis[54],
M. Veltri[22,r], A. Venkateswaran[68], M. Veronesi[32], M. Vesterinen[56], D. Vieira[65],
M. Vieites Diaz[49], H. Viemann[76], X. Vilasis-Cardona[85], E. Vilella Figueras[60], A. Villa[20],
P. Vincent[13], F.C. Volle[11], D. Vom Bruch[10], A. Vorobyev[38], V. Vorobyev[43,u], N. Voropaev[38],
K. Vos[80], R. Waldi[17], J. Walsh[29], C. Wang[17], J. Wang[5], J. Wang[4], J. Wang[3], J. Wang[73],
M. Wang[3], R. Wang[54], Y. Wang[7], Z. Wang[50], Z. Wang[3], Z. Wang[6], J.A. Ward[56,69],
N.K. Watson[53], D. Websdale[61], C. Weisser[64], B.D.C. Westhenry[54], D.J. White[62],
M. Whitehead[54], A.R. Wiederhold[56], D. Wiedner[15], G. Wilkinson[63], M. K. Wilkinson[68],
I. Williams[55], M. Williams[64], M.R.J. Williams[58], F.F. Wilson[57], W. Wislicki[36], M. Witek[35],
L. Witola[17], G. Wormser[11], S.A. Wotton[55], H. Wu[68], K. Wyllie[48], Z. Xiang[6], D. Xiao[7], Y. Xie[7],
A. Xu[5], J. Xu[6], L. Xu[3], M. Xu[56], Q. Xu[6], Z. Xu[9], Z. Xu[6], D. Yang[3], S. Yang[6], Y. Yang[6],
Z. Yang[5], Z. Yang[66], Y. Yao[68], L.E. Yeomans[60], H. Yin[7], J. Yu[71], X. Yuan[68], O. Yushchenko[44],
E. Zaffaroni[49], M. Zavertyaev[16,t], M. Zdybal[35], O. Zenaiev[48], M. Zeng[3], D. Zhang[7], L. Zhang[3],
S. Zhang[71], S. Zhang[5], Y. Zhang[5], Y. Zhang[63], A. Zharkova[83], A. Zhelezov[17], Y. Zheng[6],
T. Zhou[5], X. Zhou[6], Y. Zhou[6], V. Zhovkovska[11], X. Zhu[3], X. Zhu[7], Z. Zhu[6], V. Zhukov[14,40],
Q. Zou[4], S. Zucchelli[20,e], D. Zuliani[28], G. Zunica[62].

[1] Centro Brasileiro de Pesquisas Físicas (CBPF), Rio de Janeiro, Brazil
[2] Universidade Federal do Rio de Janeiro (UFRJ), Rio de Janeiro, Brazil
[3] Center for High Energy Physics, Tsinghua University, Beijing, China
[4] Institute Of High Energy Physics (IHEP), Beijing, China
[5] School of Physics State Key Laboratory of Nuclear Physics and Technology, Peking University, Beijing, China
[6] University of Chinese Academy of Sciences, Beijing, China
[7] Institute of Particle Physics, Central China Normal University, Wuhan, Hubei, China
[8] Univ. Savoie Mont Blanc, CNRS, IN2P3-LAPP, Annecy, France
[9] Université Clermont Auvergne, CNRS/IN2P3, LPC, Clermont-Ferrand, France
[10] Aix Marseille Univ, CNRS/IN2P3, CPPM, Marseille, France
[11] Université Paris-Saclay, CNRS/IN2P3, IJCLab, Orsay, France
[12] Laboratoire Leprince-Ringuet, CNRS/IN2P3, Ecole Polytechnique, Institut Polytechnique de Paris, Palaiseau, France
[13] LPNHE, Sorbonne Université, Paris Diderot Sorbonne Paris Cité, CNRS/IN2P3, Paris, France
[14] I. Physikalisches Institut, RWTH Aachen University, Aachen, Germany
[15] Fakultät Physik, Technische Universität Dortmund, Dortmund, Germany
[16] Max-Planck-Institut für Kernphysik (MPIK), Heidelberg, Germany
[17] Physikalisches Institut, Ruprecht-Karls-Universität Heidelberg, Heidelberg, Germany
[18] School of Physics, University College Dublin, Dublin, Ireland
[19] INFN Sezione di Bari, Bari, Italy
[20] INFN Sezione di Bologna, Bologna, Italy
[21] INFN Sezione di Ferrara, Ferrara, Italy
[22] INFN Sezione di Firenze, Firenze, Italy
[23] INFN Laboratori Nazionali di Frascati, Frascati, Italy
[24] INFN Sezione di Genova, Genova, Italy
[25] INFN Sezione di Milano, Milano, Italy
[26] INFN Sezione di Milano-Bicocca, Milano, Italy
[27] INFN Sezione di Cagliari, Monserrato, Italy
[28] Universita degli Studi di Padova, Universita e INFN, Padova, Padova, Italy
[29] INFN Sezione di Pisa, Pisa, Italy
[30] INFN Sezione di Roma La Sapienza, Roma, Italy

[31] INFN Sezione di Roma Tor Vergata, Roma, Italy

[32] Nikhef National Institute for Subatomic Physics, Amsterdam, Netherlands

[33] Nikhef National Institute for Subatomic Physics and VU University Amsterdam, Amsterdam, Netherlands

[34] AGH - University of Science and Technology, Faculty of Physics and Applied Computer Science, Kraków, Poland

[35] Henryk Niewodniczanski Institute of Nuclear Physics Polish Academy of Sciences, Kraków, Poland

[36] National Center for Nuclear Research (NCBJ), Warsaw, Poland

[37] Horia Hulubei National Institute of Physics and Nuclear Engineering, Bucharest-Magurele, Romania

[38] Petersburg Nuclear Physics Institute NRC Kurchatov Institute (PNPI NRC KI), Gatchina, Russia

[39] Institute for Nuclear Research of the Russian Academy of Sciences (INR RAS), Moscow, Russia

[40] Institute of Nuclear Physics, Moscow State University (SINP MSU), Moscow, Russia

[41] Institute of Theoretical and Experimental Physics NRC Kurchatov Institute (ITEP NRC KI), Moscow, Russia

[42] Yandex School of Data Analysis, Moscow, Russia

[43] Budker Institute of Nuclear Physics (SB RAS), Novosibirsk, Russia

[44] Institute for High Energy Physics NRC Kurchatov Institute (IHEP NRC KI), Protvino, Russia, Protvino, Russia

[45] ICCUB, Universitat de Barcelona, Barcelona, Spain

[46] Instituto Galego de Física de Altas Enerxías (IGFAE), Universidade de Santiago de Compostela, Santiago de Compostela, Spain

[47] Instituto de Fisica Corpuscular, Centro Mixto Universidad de Valencia - CSIC, Valencia, Spain

[48] European Organization for Nuclear Research (CERN), Geneva, Switzerland

[49] Institute of Physics, Ecole Polytechnique Fédérale de Lausanne (EPFL), Lausanne, Switzerland

[50] Physik-Institut, Universität Zürich, Zürich, Switzerland

[51] NSC Kharkiv Institute of Physics and Technology (NSC KIPT), Kharkiv, Ukraine

[52] Institute for Nuclear Research of the National Academy of Sciences (KINR), Kyiv, Ukraine

[53] University of Birmingham, Birmingham, United Kingdom

[54] H.H. Wills Physics Laboratory, University of Bristol, Bristol, United Kingdom

[55] Cavendish Laboratory, University of Cambridge, Cambridge, United Kingdom

[56] Department of Physics, University of Warwick, Coventry, United Kingdom

[57] STFC Rutherford Appleton Laboratory, Didcot, United Kingdom

[58] School of Physics and Astronomy, University of Edinburgh, Edinburgh, United Kingdom

[59] School of Physics and Astronomy, University of Glasgow, Glasgow, United Kingdom

[60] Oliver Lodge Laboratory, University of Liverpool, Liverpool, United Kingdom

[61] Imperial College London, London, United Kingdom

[62] Department of Physics and Astronomy, University of Manchester, Manchester, United Kingdom

[63] Department of Physics, University of Oxford, Oxford, United Kingdom

[64] Massachusetts Institute of Technology, Cambridge, MA, United States

[65] University of Cincinnati, Cincinnati, OH, United States

[66] University of Maryland, College Park, MD, United States

[67] Los Alamos National Laboratory (LANL), Los Alamos, United States

[68] Syracuse University, Syracuse, NY, United States

[69] School of Physics and Astronomy, Monash University, Melbourne, Australia, associated to [56]

[70] Pontifícia Universidade Católica do Rio de Janeiro (PUC-Rio), Rio de Janeiro, Brazil, associated to [2]

[71] Physics and Micro Electronic College, Hunan University, Changsha City, China, associated to [7]

[72] Guangdong Provincial Key Laboratory of Nuclear Science, Guangdong-Hong Kong Joint Laboratory of Quantum Matter, Institute of Quantum Matter, South China Normal University, Guangzhou, China, associated to [3]

[73] School of Physics and Technology, Wuhan University, Wuhan, China, associated to [3]

[74] Departamento de Fisica , Universidad Nacional de Colombia, Bogota, Colombia, associated to [13]

[75] Universität Bonn - Helmholtz-Institut für Strahlen und Kernphysik, Bonn, Germany, associated to [17]

[76] Institut für Physik, Universität Rostock, Rostock, Germany, associated to [17]

[77] Eotvos Lorand University, Budapest, Hungary, associated to [48]

[78] INFN Sezione di Perugia, Perugia, Italy, associated to [21]

[79] Van Swinderen Institute, University of Groningen, Groningen, Netherlands, associated to [32]

[80] Universiteit Maastricht, Maastricht, Netherlands, associated to [32]

[81] National Research Centre Kurchatov Institute, Moscow, Russia, associated to [41]

[82] National Research University Higher School of Economics, Moscow, Russia, associated to [42]

[83] National University of Science and Technology "MISIS", Moscow, Russia, associated to [41]

[84] National Research Tomsk Polytechnic University, Tomsk, Russia, associated to [41]

[85] DS4DS, La Salle, Universitat Ramon Llull, Barcelona, Spain, associated to [45]

[86] Department of Physics and Astronomy, Uppsala University, Uppsala, Sweden, associated to [59]

[87] University of Michigan, Ann Arbor, United States, associated to [68]

[a] Universidade Federal do Triângulo Mineiro (UFTM), Uberaba-MG, Brazil

[b] Hangzhou Institute for Advanced Study, UCAS, Hangzhou, China

[c] Excellence Cluster ORIGINS, Munich, Germany

[d] Università di Bari, Bari, Italy

[e] Università di Bologna, Bologna, Italy

[f] Università di Cagliari, Cagliari, Italy

[g] Università di Ferrara, Ferrara, Italy

[h] Università di Firenze, Firenze, Italy

[i] Università di Genova, Genova, Italy

[j] Università degli Studi di Milano, Milano, Italy

[k] Università di Milano Bicocca, Milano, Italy

[l] Università di Modena e Reggio Emilia, Modena, Italy

[m] Università di Padova, Padova, Italy

[n] Scuola Normale Superiore, Pisa, Italy

[o] Università di Pisa, Pisa, Italy

[p] Università della Basilicata, Potenza, Italy

[q] Università di Roma Tor Vergata, Roma, Italy

[r] Università di Urbino, Urbino, Italy

[s] MSU - Iligan Institute of Technology (MSU-IIT), Iligan, Philippines

[t] P.N. Lebedev Physical Institute, Russian Academy of Science (LPI RAS), Moscow, Russia

[u] Novosibirsk State University, Novosibirsk, Russia

[†] Deceased